A natural variation-based screen in mouse cells reveals USF2 as a regulator of the DNA damage response and cellular senescence

Taekyu Kang[1,2], Emily C. Moore[3], Emily E. K. Kopania[3], Christina D. King[1], Birgit Schilling[1], Judith Campisi[1], Jeffrey M. Good[3], and Rachel B. Brem[1,2*]

[1]Buck Institute for Research on Aging, Novato, CA; [2]Department of Plant and Microbial Biology, UC Berkeley, Berkeley, CA; [3]Division of Biological Sciences, University of Montana, Missoula, MT

*Correspondence: rbrem@berkeley.edu

Abstract

Cellular senescence is a program of cell cycle arrest, apoptosis resistance, and cytokine release induced by stress exposure in mammalian cells. Landmark studies in laboratory mice have characterized a number of master senescence regulators, including $p16^{INK4a}$, p21, NF-kB, p53, and C/EBPβ. To discover other molecular players in senescence, we developed a screening approach to harness the evolutionary divergence between mouse species. We found that primary cells from the Mediterranean mouse *Mus spretus,* when treated with DNA damage to induce senescence, produced less cytokine and had less-active lysosomes than cells from laboratory *M. musculus.* We used allele-specific expression profiling to catalog senescence-dependent *cis*-regulatory variation between the species at thousands of genes. We then tested for correlation between these expression changes and interspecies sequence variants in the binding sites of transcription factors. Among the emergent candidate senescence regulators, we chose a little-studied cell cycle factor, USF2, for molecular validation. In acute irradiation experiments, cells lacking USF2 exhibited compromised DNA damage repair and response. Longer-term senescent cultures without USF2 mounted an exaggerated senescence regulatory program—shutting down cell cycle and DNA repair pathways, and turning up cytokine expression, more avidly than wild-type. We interpret these findings under a model of pro-repair, anti-senescence regulatory function by USF2. Our study affords new insights into the mechanisms by which cells commit to senescence, and serves as a validated proof of concept for natural variation-based regulator screens.

Introduction

Mammalian cells of many types, upon exposure to stress, can enter a senescence program, in which they stop dividing, become refractory to apoptosis, and release soluble inflammation and tissue remodeling factors termed the senescence-associated secretory phenotype (SASP) (1–4). The resulting acute immune response can clear debris, promote wound healing, and/or suppress tumorigenesis (5–8). However, during aging, senescent cells can remain long past any initial triggering event, resulting in chronic inflammation that damages the surrounding tissue (5,9–12). Landmark work has revealed the benefits of eliminating senescent cells to treat age-related pathologies and boost median lifespan (7,8,13,14).

Establishment of the senescent state and the activity of senescent cells hinge in large part on gene regulatory events. Finding molecular players that control this process is an active area of research. Now-classic work has implicated $p16^{INK4a}$ and p21 in the repression of pro-cell cycle genes and promotion of growth arrest (15) after DNA damage, and NF-kB, p53, and C/EBPβ (16) as regulators of the SASP. However, given the complexity of the senescence program, many more regulators likely remain to be identified. Indeed, bioinformatic approaches have identified dozens of other transcription factor candidates in senescence (17–24), many of which remain unvalidated (but see (18–21) for recent discoveries of the roles of DLX2, FOXO3 and AP-1 in senescence).

We set out to develop a novel approach to survey transcription factors that play a role in cellular senescence, with the potential for increased specificity relative to traditional genomic screens. Our strategy took advantage of the natural genetic variation in senescence gene expression, and transcription factor binding sites, across mouse species. Among the top hits from this

analysis, we chose the under-studied factor USF2 for validation experiments, focusing on gene regulation and cellular phenotypes during senescence induction and maintenance.

Results

A dampened senescence program in primary fibroblasts of *Mus spretus*

We initiated our study on the premise that senescent phenotypes could differ among mouse lineages, and that these changes could serve as a tool to uncover novel regulators. Toward this end, we first characterized the dependence of senescent phenotypes on genotype. We isolated primary tail fibroblasts from PWK, a wild-derived purebred strain of *Mus musculus,* and from the wild-derived, purebred STF strain of the Mediterranean mouse species *M. spretus*. We treated each with ionizing radiation, incubated to allow development of senescence (3,25,26), and assessed features of the resulting senescent cells, with untreated cells as controls. Such cultures from both species arrested growth and exhibited a flattened and enlarged morphology (Figure 1A), as expected if both cultures had entered the senescent state (26). By contrast, assays of senescence-associated β-galactosidase activity, a senescence biomarker (27), revealed a marked difference between the cultures, with two to eight-fold lower staining in *M. spretus* cells relative to *M. musculus* cells (Figure 1B).

To explore further the divergence in senescent phenotypes between cells of our focal species, we profiled bulk RNA levels in senescent and control primary fibroblast cultures from each species (Supplemental Table S1). We inspected genes of the SASP immune-stimulatory program (4), and found that this gene cohort was induced more highly in *M. musculus* cells than in those of *M. spretus* during senescence (Figure 2A). Likewise, in an unbiased search of Gene

Ontology terms, we identified several suites of immune response and NF-κB signaling genes that were enriched for senescence-specific differential expression between the cultures. In each case, the gene groups were more strongly induced during senescence in *M. musculus* cells than in *M. spretus* cultures (Figure 2B and Supplemental Tables S2 and S3); among members of the latter we noted *Cxcl1* (28), *Il6* (29), *Ccls* 2,7 and 8 (30), *Mmp13* (31), and other reported SASP genes (Supplemental Figure S1). These data make clear that, at the level of mRNA, the senescence regulatory program differs markedly between fibroblasts of our focal species.

We hypothesized that much of the divergence between *M. musculus* and *M. spretus* cells during senescence, which we detected in RNA measurements, would result in differential protein abundance. In pursuing this notion, we focused on proteins secreted into the medium by senescent cells, owing to the physiological importance of the SASP (30). We collected conditioned media from senescent and control cultures of primary fibroblasts of each genotype, and we used it as input into unbiased mass spectrometry to quantify protein abundance. The results revealed an overall increase in the secretion of common SASP components, including CCL chemokines, matrix metalloproteases, and serpins, in senescent *M. musculus* cells relative to those of *M. spretus* (Figure 2C, Supplemental Figure S2, and Supplemental Table S4). Together, our characterization experiments show that *M. spretus* fibroblasts enter a senescent growth arrest similar to that of *M. musculus* fibroblasts, but with expression of certain SASP factors spiking less highly.

A genomic screen for senescence transcription factors using *cis*-regulatory sequence variations

Having established divergence between *M. musculus* and *M. spretus* primary fibroblasts in senescence mRNA and protein secretion (Figures 1 and 2), we reasoned that such differences could be harnessed in an *in silico* screen for senescence regulators. We designed an analysis focused on gene regulation—in particular, on variation between the species at the binding sites of transcription factors (Figure 3A). We expected that, at some genes, *cis*-regulatory elements encoded in the *M. musculus* genome would drive expression during senescence differently than those in the *M. spretus* genome. We reasoned that if *cis*-acting variation effects were enriched among the loci bound by a given transcription factor across the genome, the signal could be interpreted as a signpost for the factor's activity during senescence (Figure 3A). In this way, all *cis*-regulatory variants between the species that manifested in cultured primary fibroblasts, whether of large or small effect size, and regardless of their potential for phenotypic impact, could contribute to the search for transcription factors relevant for senescence.

As a resource for this approach, we mated PWK *M. musculus* and STF *M. spretus* to yield F1 hybrid animals from which we derived primary tail fibroblasts for culture and irradiation. These *M. musculus* x *M. spretus* F1 hybrid fibroblasts, when irradiated, exhibited a flattened morphology reflecting entry into senescence; senescence-associated β-galactosidase activity was of a magnitude between those of purebred *M. musculus* and *M. spretus* fibroblasts upon irradiation (Supplemental Figure S3). We subjected senescent and control F1 hybrid fibroblasts to RNA-seq profiling, and we used the results to quantify levels of transcripts derived from the *M. musculus* and *M. spretus* alleles of each gene in each condition (Supplemental Table S1). At a given gene, any difference between allele-specific expression in an F1 hybrid can be attributed to variants inherited from the parent species that perturb gene regulation in *cis* at the locus, because *trans*-acting factors impinge to the same extent on both alleles (32). Analyzing the response to senescence induction for a given gene, we found that the allele-specific expression difference between the alleles in the F1 hybrid was a partial predictor of the

expression divergence between the *M. musculus* and *M. spretus* purebreds, in our primary cell system (Supplemental Figure S4). The latter trend reflects the joint contributions of *cis*- and *trans*-acting variants to total expression divergence between the species, as expected (33). Separately, to survey overall regulatory programs in F1 hybrid primary fibroblasts, we formulated the expression level of a given gene in a given condition as the sum of the measured levels of the *M. musculus* and *M. spretus* alleles. In this analysis, focusing on SASP genes as we had done for the purebreds (Figure 2A), we found that the expression program of senescent F1 hybrid cells was, for most genes, intermediate between the low levels seen in *M. spretus* cells and the high levels in *M. musculus* (Supplemental Figure S5). These data indicate that *M. musculus* x *M. spretus* F1 hybrid fibroblasts do not exhibit heterosis with respect to senescence-associated genes, and do manifest extensive, senescence-dependent *cis*-regulatory variation.

We next used the expression measurements from F1 hybrid cells as input into our *in silico* screen to identify senescence-dependent transcription factor activity. For a given transcription factor, we collated binding sites detected by chromatin immunoprecipitation upstream of genes across a panel of tissues (34). At each site, we tabulated the presence or absence of DNA sequence variants in the respective genomes of *M. musculus* and *M. spretus*. We then tested whether, across the genome, genes with these binding site variants were enriched for senescence-associated expression differences between the two alleles in the F1 hybrid. This test had the capacity for high power to detect even subtle contributions from transcription factors if they had deep binding-site coverage in the input data; five factors attained genome-wide significance (Figure 3B and Supplemental Table S5). Among them, PBX1 (35) and CREBBP (36,37) were previously implicated in cellular senescence, providing a first line of evidence for the strength of our approach to identify signatures of condition-dependent transcription factor function. The top-scoring transcription factor in our screen, a basic-helix-loop-helix leucine-zipper protein called upstream stimulatory factor 2 (USF2; Figure 3B-C), had not been

experimentally characterized in stress response or senescence. However, classic studies had established USF2 as a regulator of the cell cycle and tumor suppression (38–41). More recently, USF2 was shown to control cytokine release in immune cells (42). Considering these known functions, and bioinformatic analyses suggesting a link between USF2 and senescence programs (21), we chose USF2 for in-depth validation. In detailed genomic tests, single variants between *M. musculus* and *M. spretus* at USF2 binding sites drove most of the relationship with allele-specific expression in hybrid senescent cells (Figure 3D). These variants were over-represented at positions central to, and slightly downstream of, experimentally determined peaks for USF2 (Figure 3E), highlighting the likely importance of this region in USF2's mechanisms of binding and regulation.

USF2 modulates cell proliferation and the acute DNA damage response

Our question at this point was whether and how USF2 regulated senescence programs. As such, we shifted our focus from natural genetic variation to controlled, laboratory-induced genetic perturbations in a single genetic background. We designed two short hairpin RNAs (shRNAs) targeting *Usf2*, each in a lentiviral vector under the U6 promoter. Expression measurements upon transformation of PWK *M. musculus* primary tail fibroblasts confirmed 2.5 and 3-fold knockdown of *Usf2* expression, respectively, from these shRNAs (Supplemental Figure S6). We developed two experimental workflows using these shRNAs. One approach aimed to define the role of USF2 in the acute DNA damage response (Figure 4A) and establishment of senescence (Figure 5A): we infected cells with *Usf2* shRNAs, cultured them under standard conditions, and then induced senescence by irradiation. In a second approach, we focused on the function of USF2 in maintenance of senescence, inducing senescence in wild-type cells and knocking down *Usf2* afterward (Figure 5C).

Given that our first experimental design used *Usf2* knockdown in cells under standard conditions to study the irradiation response and senescence (Figures 4A and 5A), we began by characterizing the effects of reduced *Usf2* expression in resting cells. Uptake of the nucleotide analog EdU, a marker of DNA synthesis, was reduced by 40% in resting primary fibroblasts expressing the *Usf2* shRNA relative to scrambled shRNA controls (Supplemental Figure S7). Transcriptional profiling of these resting cultures (Supplemental Table S6), followed by functional-genomic (Gene Ontology) analyses, revealed enrichment for biosynthesis, development, cell growth, and DNA repair terms altered upon *Usf2* knockdown relative to controls (Supplemental Table S7). These data support a role for USF2 in wild-type growth and housekeeping gene expression programs in untreated primary fibroblasts, consistent with studies of USF2 in cell growth in other tissues and contexts (26,38–41). Our results in resting cells also provide a first indication of the potential function of USF2 in the DNA damage response.

We next directly pursued the importance of USF2 during the acute response to irradiation (Figure 4A). DNA damage signaling, an inducer of cellular senescence (2,3), drops sharply in intensity within eight hours and then more gradually over several day after irradiation (43), culminating in a lower persistent signal (44–47). We focused on the early phase of this process (six hours after irradiation) in cultures of primary fibroblasts expressing *Usf2* shRNAs or scrambled shRNA controls. Transcriptional profiling followed by Gene Ontology analyses identified gene groups enriched for expression changes dependent on condition and USF2 (Figure 4B and Supplemental Tables S6 and S8). Most salient was a trend of pervasive repression transcriptome-wide six hours after irradiation, which was detected in control cells as expected (48,49), and was blunted in cells with *Usf2* knocked down. The latter effect was particularly enriched in the transcriptional machinery, repressors of apoptosis, and several cell proliferation regulators (Figure 4B-C and Supplemental Figure S8A). We also inspected the few

top-scoring gene groups that were induced by irradiation in control cultures. These gene groups reached even higher expression levels in *Usf2* knockdown cells; notable among them was the EGFR pathway (Figure 4B and 4D and Supplemental Figure S8B), a determinant of entry into senescence in some contexts (50). DNA repair genes, a likely target for changes upon irradiation, are regulated primarily at the post-transcriptional level (51,52), and we did not detect effects of *Usf2* knockdown on their transcripts (Supplemental Figure S9).

We hypothesized that *Usf2* knockdown during the acute DNA damage response would also have cell-physiological effects. Assays of EdU incorporation to report on DNA synthesis showed effects of *Usf2* knockdown after irradiation to the same degree as in resting cultures (Supplemental Figure S7). To focus on phenotypes more proximal to DNA damage, we used the neutral comet assay (53) to measure DNA double-stranded breaks on a per-cell basis. In this setup, *Usf2* depletion increased comet tail moments by 50% six hours after irradiation, with an effect that was similar, though of smaller magnitude, in resting cell controls (Figure 4E). Next, we tracked foci of phosphorylated histone H2AX (γH2AX) in fibroblasts as a marker of chromatin decondensation, preceding the repair of DNA double-stranded breaks (54). Cells harboring *Usf2* shRNAs exhibited 30% fewer γH2AX foci than cells of the control genotype, six hours after irradiation (Figure 4F). These data establish a role for USF2 in the response to irradiation, with knockdown of this factor compromising cells' ability to mount the classical transcriptional program under this stress, and to carry out DNA damage repair.

USF2 tunes the commitment to senescence

Having knocked down *Usf2* in naïve PWK primary fibroblasts and irradiated them to study the acute DNA damage response, we now allowed the irradiated cultures to enter senescence

(Figure 5A). Growth arrest and flattened morphology were indistinguishable between these cells and controls harboring scrambled shRNAs (see Figure 5G), indicating that wild-type levels of *Usf2* were not required at the point of irradiation to establish senescence *per se*. To investigate quantitative characteristics of these senescent cultures, we subjected them to expression profiling and Gene Ontology enrichment analyses (Supplemental Tables S6 and S9). Among top-scoring gene groups, the most dramatic effects were in those that dropped in expression in senescent cultures of the control genotype, which as expected (17,55) included cell cycle and DNA repair pathways (Figure 5B and Supplemental Table S9). mRNA levels of the latter were even lower in senescent cells that had been irradiated after *Usf2* knockdown, showing a reduction of ~20% on average (Figure 5B). Among the genes of this cohort, some of which declined in expression by >5-fold with *Usf2* knockdown in senescence (Figure 5F), we noted cell cycle regulators (*Ccna2*, *Cdc20*, *Cdk1),* kinesin components (*Kif2c, Knl1*), the DNA polymerase *Pole,* and the DNA damage checkpoint ubiquitin ligase *Uhrf1* (Supplemental Figure S10A). We conclude that genes of the cell cycle and DNA repair machinery are detectable at a low but non-zero expression level in wild-type senescent cells, and that these pathways are subject to further reduction when *Usf2* is limiting.

Next, we inspected the impact of *Usf2* knockdown on inflammation and immune recruiting factors, another set of processes that had emerged from our Gene Ontology analyses of expression (Supplemental Table S9). Cells of the control genotype induced these pathways during senescence, as expected (2,3,9,29,56,57); in cells reaching senescence after *Usf2* knockdown, induction of inflammatory factors was amplified by ~10% on average (Figures 5B and 5E, and Supplemental Figure S10B). Similarly, in assays of the β-galactosidase senescence marker, we observed a modest, though robustly significant, increase in cells subject to *Usf2* knockdown and senescence treatment (Figure 5G). Together, our profiling data establish that irradiation of primary fibroblasts with reduced *Usf2* expression leads to a

quantitatively perturbed, exaggerated senescent state, with reduced expression of proliferation and DNA repair pathways, and elevated pro-inflammatory gene expression and β-galactosidase activity.

We reasoned that the changes in senescence we had seen upon irradiation of *Usf2*-depleted cells could constitute, in part, effects from increased DNA damage in the knockdown genotype (Figure 4). To pursue the role of USF2 in senescence more directly, we used our second experimental paradigm: we irradiated wild-type cells, incubated them for 10 days to allow establishment of senescence, then expressed shRNAs targeting *Usf2,* followed by 10 additional days of incubation and transcriptional profiling (Figure 5C). In control cells (harboring a scrambled shRNA), we observed expression changes for many genes from the resting state through irradiation and early and late senescence (Supplemental Tables S6 and S10, and Supplemental Figure S11), attesting to the dynamics of senescence across this timecourse as expected (17,55). Next we focused on cultures subject to *Usf2* knockdown during late senescence. The latter manifested quantitative changes largely paralleling those in cells with *Usf2* knocked down at the start of the experiment. Thus, on average, cell cycle and DNA repair genes, repressed in control cells during senescence, were expressed at even lower levels when *Usf2* was knocked down midway through the senescence time course (Figures 5D and 5F, Supplemental Tables S6 and S11, and Supplemental Figure S10A), analogous to our findings upon early knockdown of *Usf2*. Likewise, inflammatory response factors, induced during senescence in the control setting, were more highly expressed when *Usf2* was depleted after senescence establishment, as seen in our early-knockdown design (Figures 5D and 5E, Supplemental Tables S6 and S11, and Supplemental Figure S10B). We noted a handful of genes for which early *Usf2* knockdown effects were not recapitulated in our paradigm of knockdown after senescence entry (*e.g. Adamts1* and *Rarres2* in Supplemental Figure S10B). Overall, however, our analyses establish USF2 as a senescence regulator at least in part

independent of its role in the acute DNA damage response, such that in its absence, cells commit even more strongly to the senescent state.

Discussion

Complex regulatory networks likely underlie many of the quantitative behaviors of senescent cells, including kinetics and dependence on cell type and inducer (15,17,25,58,59). Exactly how these nuances are encoded remains poorly understood. In this study, we pioneered the use of interspecies genetic divergence to screen for components of the senescence regulatory machinery. This strategy complements previous studies of transcription factor binding sites in genes of the senescence program in a single genetic background (17,21). Our approach harnesses the correlation between interspecies variation in sequence and expression levels, as an additional line of evidence for senescence-specific regulatory functions by a given factor. This paradigm parallels similar tools previously used to dissect divergence in expression (60,61) and transcription factor binding (62,63) in other contexts. Broadly speaking, these methods are not highly powered for pathways under strong evolutionary constraint, which, by definition, will not vary enough among species to yield the raw observations that would go into a screening pipeline. Rather, we expect the natural variation-based approach to work best for discovering less-constrained modifiers, many of which may confer layers of quantitative regulation onto a master regulatory pathway.

We focused our experimental validation on one such modifier, the transcription factor USF2. By tracing USF2's function in proliferation and genome-wide expression in untreated cells, we extended conclusions from studies of USF2 in tumor suppression and cell cycle regulation (38–40,42), apoptosis (64) and ERK1/2 signaling (65). In an acute DNA damage setting, we

discovered that USF2 is required for cells to mount DNA repair and downstream DNA damage responses. And in senescence proper, we showed that USF2 acts as a repressor, such that in its absence, the senescence program—shutoff of cell proliferation and DNA repair, and induction of cytokines—is amplified. A compelling model is thus that even long after damage exposure, cells have access to expression states along a continuum of commitment to senescence, and that USF2 acts to help determine which state they occupy. If so, USF2 would take a place among a network of factors, including p53, ING, Rb (66,67), p21 (68,69), and p16 (70), that govern the choice between senescence, apoptosis, and repair and proliferation, depending on cell type (66) and the amount of damage or stress incurred (67).

As a corollary of these conclusions from expression profiling, we note that cell cycle and DNA repair genes, classically known to be repressed during senescence (17,55), did not hit a floor of expression in senescent cultures: we could detect them at even lower expression levels upon *Usf2* knockdown. Since our cultures comprise >99% arrested cells within several days of irradiation (see Methods), the emerging picture is that the proliferation machinery is maintained at non-zero levels even in such a population. Any ability of these gene products to reattain activity could be of particular interest as a potential mediator of the return to proliferation seen among senescent cells in certain scenarios (71,72).

Our work leaves open the mechanisms by which USF2 exerts its effects in the DNA damage response and cellular senescence. It is tempting to speculate that USF2 ultimately works in these processes in concert with its better-studied family member, USF1. Indeed, USF1 has been implicated in DNA repair (73), inflammation (74,75), immune responses (76), and p53-mediated cell cycle arrest (77) in contexts other than senescence. In addition, given that USF2 has been implicated in the TGFβ-p53 axis in apoptosis (64) and fibrosis (78), the latter pathway could mediate some part of the USF2 effects we have seen. Furthermore, regulatory network

reconstruction (Supplemental Table S12) suggests that USF2 acts upstream of several other transcription factors (KLF3, GLI3, NFIL3) with direct targets in DNA repair, DNA damage response and senescence pathways.

Alongside our use of *cis*-regulatory variation between mouse species as a screening tool for senescence genes, we also characterized overall patterns of divergence between *M. spretus* senescent cells and those of *M. musculus*. Given that the former exhibited lower levels of SASP mRNAs and proteins, we suggest that the rheostat of the senescence response is at a higher set point in this species, such that at a given level of stress (*e.g.* the irradiation we study here), cells of this species synthesize and secrete less of the SASP. We further hypothesize that this down-tuning might be a proximal cause for the lower senescence-associated β-galactosidase activity we have seen in *M. spretus* cells. Such a link would follow from current models of the senescent state in which production and secretion of SASP components (79) leads to proteotoxic stress from insoluble aggregates (80,81), an increase in the number and size of lysosomes (82), and enhanced β-galactosidase activity (83). Plausibly, any of the phenotypes we study here in cell culture could have consequences *in vivo*, with potential links to the stress- and pathogen-resistance phenotypes characterized in *M. spretus* (84–88). Together, our findings attest to the power of natural variation-based-approaches—to survey the differences that evolution has wrought over long timescales, and as a tool for molecular discoveries of relevance in any one genetic background.

Methods

Primary cell extraction and culture

Wild-derived, inbred lines of *Mus musculus* (PWK/PhJ) and *Mus spretus* (STF/Pas) and their interspecies F1 hybrids (*M. musculus* x *M. spretus*) were maintained in standard conditions under Montana Institutional Animal Care and Use Committee protocol number 062-1JGDBS-120418. Animals aged 3 to 5 months were humanely euthanized prior to tissue collection via CO_2 treatment and cervical dislocation. Five tails from each genotype were collected into chilled Dulbecco's Modified Eagle Medium (DMEM) and shipped to the Buck Institute for further processing. Metadata for the mice used in this experiment is provided in (Supplemental Table S13). Primary tail fibroblasts were extracted from the cuttings essentially as described (89). Briefly, tail cuttings first were soaked in 70% ethanol for 5 minutes and then laid out in sterile 10 cm tissue culture dishes in a biosafety cabinet for 5 minutes to dry. The tails were then transferred to a 10-cm dish containing 10 mL of complete medium (RPMI 1640 medium, 10% fetal bovine serum, 50 µM 2-mercaptoethanol, 100 µM asparagine, 2 mM glutamine, and 1% penicillin-streptomycin). Hair was removed from the tails using sterile forceps and razor blade, and the tails were cut into 2-3 mm pieces using sterile surgical scissors. These pieces were then transferred into a 2 mL cryotube containing a collagenase D–pronase solution and left in a shaking incubator at 37ºC for 90 minutes. Following incubation, the contents of the cryotubes were placed into a 70 µm cell strainer in a new 10-cm dish containing 10 mL of compete medium. Using the back end of a sterile 10 mL syringe plunger, the tissue was ground into the strainer for 5-10 minutes to release the cells into the media. The cell suspension was then collected into 15 mL conical tubes and centrifuged at 580 x g and 4ºC for 5 minutes. The supernatant was removed and replaced with fresh complete medium, and the centrifugation was repeated for two additional rounds. After the final spin, the media was replaced with complete medium supplemented with 250 ng/mL of amphotericin B. The cell suspension was placed in a 10-cm dish and incubated in a 37ºC humidified incubator at 3% O_2 and 10% CO_2 for two days before passage and continued culture in complete medium (DMEM, 10% FBS, 1% penicillin-streptomycin). This complete medium was used for the remainder of our experiments. For long

term storage, cells were suspended in 5% DMSO in FBS, aliquoted into cryotubes, and placed in a slow cooling container in a -80ºC freezer overnight. The following day, the cryotubes were moved out of the slow cooling container and placed into long term containers in the freezer. To thaw cells for continued culture, cryotubes containing frozen aliquots were swirled in a 37ºC water bath until only a thin layer of ice remained in the vial. The contents of the cryotube were then immediate transferred into a flask containing pre-warmed complete medium and incubated overnight. The following day the cells were washed twice with PBS to remove any trace of DMSO and cultured in complete medium. For experiments in wild-type *M. musculus*, *M. spretus*, and F1 hybrid cells we considered the culture from each individual animal to represent one biological replicate of the respective genotype. In knockdown experiments (see below) we carried out infection of two such cultures with each shRNA-bearing virus, which we refer to as biological replicates. In either setup, we refer to the split cultures from a given biological replicate as technical replicates in a given assay.

Irradiation treatment

To treat a given cell culture replicate with ionizing radiation (3,25,26) for a cell-biological assay or omics profiling, we proceeded as follows. The day before irradiation, cells were seeded at 60-70% confluency and incubated in a 37ºC humidified incubator at 3% O_2 and 10% CO_2 overnight in complete medium. The next day, a subset of cells was collected and used as input into the respective experiment as the unirradiated control. The remainder of the culture was transferred into an X-RAD 320 X-Ray Biological Irradiator and treated with 15 Gy of X-ray irradiation. Cultures were then placed back into the 37ºC humidified incubator at 3% O_2 and 10% CO_2 until sampling at 6 hours for marker assays and RNA-seq focused on acute DNA damage response, or 7, 10 or 20 days for marker assays and RNA-seq and proteomics focused

on senescence (in which case the medium was replaced 6-8 hours after irradiation, then every 48 hours for the remainder of the experiment), as detailed below.

Senescence marker assays

For a given replicate culture after irradiation and incubation (see above), senescence-associated β-galactosidase activity was measured using the BioVision Inc. Senescence Detection Kit (cat. #K320): cells were fixed, permeabilized, and incubated with the staining solution containing X-gal overnight. Multiple images were taken the following day using a brightfield microscope, and the image names were randomized before the proportion of β-galactosidase-positive cells was counted manually to remove potential sources of bias. Cultures were considered to be senescent if they showed less than 10% EdU incorporation (see below) and over 90% β-galactosidase-positive cells. In the species comparison of Figure 1 we subjected two technical replicate cultures of each of three biological replicates per purebred species to irradiation (see above) followed by β-galactosidase assays at the indicated timepoints. In Supplemental Figure S3, data for purebreds were from Figure 1 at day 7; separately, for the interspecies F1 hybrid, we carried out irradiation and β-galactosidase assays as above for two technical replicates from one biological replicate. In Figure 5G, we carried out irradiation and β-galactosidase assays as above at day 7 after irradiation for two technical replicates from each of two biological replicates of *M. musculus* cells infected with lentivirus harboring the scrambled control and two of each *Usf2* knockdown (see below).

RNA collection and sequencing

For a given replicate culture of a given genotype, either before irradiation or 6 hours, 10 days, or 20 days after irradiation (see above), cells were treated with TRIzol™ and RNA was extracted using chloroform and ethanol precipitation. The RNA was then further purified using the Qiagen RNeasy Kit (cat. #74004) for DNase treatment and column cleanup. The purity of the extracted RNA was verified using a NanoDrop ND-1000 Spectrophotometer; all samples had 260/280 and 260/230 ratios greater than 2.0. Purified RNA in distilled RNase/DNase free water was snap frozen using dry ice and stored at -80°C. Samples were then either transferred to the QB3 Genomics core at University of California, Berkeley for library prep and sequencing on 150PE NovaSeq S4 or shipped to Novogene Co. (Sacramento, CA) for the same. Both facilities provided 25 million paired end reads per sample. For expression profiles of purebred cells and *M. musculus* x *M. spretus* F1 hybrid cells, we subjected three biological replicates of a given genotype to irradiation (see above) followed by RNA-seq at the indicated timepoints. To assess transcriptional impacts of *Usf2* knockdown we carried out irradiation and RNA isolation as above for two biological replicates of *M. musculus* cells infected with lentivirus harboring the scrambled control and two of each *Usf2* knockdown (see below).

Pseudogenome and VCF generation

As publicly available annotations for *M. musculus* and *M. spretus* are in the context of their reference genomes (GRCm38.96 and SPRET_EiJ_v1.96 respectively), custom pseudogenomes for strains PWK and STF were generated and used for this study. For the PWK pseudogenome, variant calls between PWK and the reference genome in the form of a variant call file (VCF) were downloaded from the Sanger Mouse Genomes Project database (https://www.sanger.ac.uk/data/mouse-genomes-project/). A pseudogenome using the VCF and the GRCm38.96 reference genome was created using bcftools v1.9 (90). To generate shotgun sequence data for the STF pseudogenome, DNA was extracted from *M. spretus* liver

tissue using Qiagen DNeasy spin columns (cat. #69506). The sample was sheared via sonication (Covaris E220), and prepared using the New England Biolabs NEBNext Ultra DNA Library kit (cat. #E7370L). The final library was sequenced on a single lane of 150bp PE Illumina HiSeq X at Novogene, Inc. The latter reads were aligned to the SPRET_EiJ_v1.96 reference genome using bowtie v2.2.3 (91), and a VCF was generated using bfctools mpileup and filtered for quality, depth, and SNPs using vcfutils (92,93). The VCF was then used with the reference genome to create a STF pseudogenome using bcftools. The pseudogenomes were verified by identifying a number of called variants by hand. A VCF of variants between the STF and PWK pseudogenomes was generated as above aligning the STF whole genome sequencing reads to the PWK pseudogenome.

RNA-seq processing

In transcriptional profiles of *M. musculus* x *M. spretus* F1 hybrid cells, sequencing reads from a given replicate were aligned to a concatenated PWK/STF pseudogenome using tophat v2.1.1 (94) allowing for zero mismatches to ensure allele specific mapping. Alignments were then filtered for uniquely mapped reads using samtools v1.3.1, and gene counts were generated using HTSeq v0.11.2 (95) and genome annotations (GRCm38.96, SPRET_EiJ_v1.96) for both species from Ensembl. Counts were then converted to transcripts per million (TPM) using custom R scripts, and genes were filtered for those showing counts in more than half the samples sequenced.

In transcriptional profiles of purebred *M. musculus* wild-type cells and *M. musculus* cells infected with lentiviruses harboring shRNAs, RNA-seq processing was as above but mapping was to the PWK pseudogenome only; for profiles of purebred *M. spretus* wild-type cells, mapping was to the STF pseudogenome only.

Data for the average TPM across biological replicates for purebred parents and interspecific F1 hybrid are reported in Supplemental Table S1. Average TPM across biological replicates for shRNA-treated *M. musculus* cells are reported in Supplemental Table S6.

Gene Ontology enrichment analysis of RNA-seq data

For the comparison of transcriptional profiles of *M. musculus* and *M. spretus* purebred cells, for each gene in turn we tabulated the average TPM count from each species across replicates, and then took the $\log_2$ of the ratio of these averages, $r_{sen,true}$. We downloaded Gene Ontology annotations from the AmiGO 2 (96,97) database and filtered for those with supporting biological data. For each term, we summed the $r_{sen,true}$ values across all genes of the term, yielding $s_{sen,true}$. To assess the enrichment for high or low values of this sum, we first took the absolute value, $|s_{sen,true}|$. We then sampled, from the total set of genes with expression data, a random set of the same number as that in the true data for the term; we calculated the species difference $r_{sen,rand}$ for each such gene and the absolute value of the sum over them all, $|s_{sen,rand}|$. We used as a *p*-value the proportion of 10,000 resampled data sets in which $|s_{sen,true}| > |s_{sen,rand}|$.

For analysis of the impact of *Usf2* knockdown on expression before or 6 hours, 10 days, or 20 days after irradiation (see below), Gene Ontology enrichment tests were as above except that we took the ratio, for a given gene, between the average expression in purebred *M. musculus* (PWK) cells infected with lentivirus harboring scrambled shRNA and the analogous quantity across both *Usf2*-targeting shRNA treatments.

Proteomic analysis of secreted proteins

Conditioned medium preparation. For a given replicate culture, either before irradiation or 10 days after irradiation (see above), cells were washed three times with PBS and incubated with serum and phenol red free DMEM containing 1% pen-strep for 24 hours. The following day the conditioned medium was collected and passed through a 0.45 µm filter to remove cellular debris. The conditioned medium was placed in a -80°C freezer for storage before use as input into proteomic profiling (see below). For proteomic profiles of purebred cells, we carried out this procedure for three technical replicate cultures of one biological replicate per species.

Sample concentration. 30 mL of conditioned media for each replicate were concentrated to 400 µL with 15 mL 3 kDa filters (Millipore Sigma, Burlington, MA). Protein concentration was determined using the Bicinchoninic Acid (BCA) assay (Thermo Fisher Scientific, Waltham, MA).

Protein digestion and desalting. Aliquots of 200 µg protein lysates for each sample were brought to the same overall volume of 52 µL with water, reduced using 20 mM dithiothreitol in 50 mM triethylammonium bicarbonate buffer (TEAB) at 50°C for 10 min, cooled to room temperature (RT) and held at RT for 10 min, and alkylated using 40 mM iodoacetamide in 50 mM TEAB at RT in the dark for 30 min. Samples were acidified with 12% phosphoric acid to obtain a final concentration of 1.2% phosphoric acid. S-Trap buffer consisting of 90% methanol in 100 mM TEAB at pH ~7.1, was added and samples were loaded onto the S-Trap mini spin columns. The entire sample volume was spun through the S-Trap mini spin columns at 4,000 x g and RT, binding the proteins to the mini spin columns. Subsequently, S-Trap mini spin columns were washed twice with S-Trap buffer at 4,000 x g at RT and placed into clean elution tubes. Samples were incubated for one hour at 47°C with sequencing grade trypsin (Promega, San Luis Obispo, CA) dissolved in 50 mM TEAB at a 1:25 (w/w) enzyme:protein ratio. Afterwards, trypsin solution was added again at the same ratio, and proteins were digested overnight at 37°C.

Peptides were sequentially eluted from mini S-Trap spin columns with 50 mM TEAB, 0.5% formic acid (FA) in water, and 50% acetonitrile (ACN) in 0.5% FA. After centrifugal evaporation, samples were resuspended in 0.2% FA in water and desalted with Oasis 10 mg Sorbent Cartridges (Waters, Milford, MA). The desalted elutions were then subjected to an additional round of centrifugal evaporation and re-suspended in 0.2% FA in water at a final concentration of 1 µg/µL. Subsequently, 8 µL of each sample were diluted with 2% ACN in 0.1% FA to obtain a concentration of 400 ng/µL. Finally, 1 µL of indexed Retention Time Standard (iRT, Biognosys, Schlieren, Switzerland) was added to each sample, thus bringing up the total volume to 20 µL (98).

Mass spectrometric analysis. Reverse-phase HPLC-MS/MS analyses were performed on a Dionex UltiMate 3000 system coupled online to an Orbitrap Exploris 480 mass spectrometer (Thermo Fisher Scientific, Bremen, Germany). The solvent system consisted of 2% ACN, 0.1% FA in water (solvent A) and 80% ACN, 0.1% FA in ACN (solvent B). Digested peptides (400 ng) were loaded onto an Acclaim PepMap 100 C_{18} trap column (0.1 x 20 mm, 5 µm particle size; Thermo Fisher Scientific) over 5 min at 5 µL/min with 100% solvent A. Peptides (400 ng) were eluted on an Acclaim PepMap 100 C_{18} analytical column (75 µm x 50 cm, 3 µm particle size; Thermo Fisher Scientific) at 300 nL/min using the following gradient: linear from 2.5% to 24.5% of solvent B in 125 min, linear from 24.5% to 39.2% of solvent B in 40 min, up to 98% of solvent B in 1 min, and back to 2.5% of solvent B in 1 min. The column was re-equilibrated for 30 min with 2.5% of solvent B, and the total gradient length was 210 min. Each sample was acquired in data-independent acquisition (DIA) mode (99–101), in triplicates. Full MS spectra were collected at 120,000 resolution (Automatic Gain Control (AGC) target: 3e6 ions, maximum injection time: 60 ms, 350-1,650 *m/z*), and MS2 spectra at 30,000 resolution (AGC target: 3e6 ions, maximum injection time: Auto, Normalized Collision Energy (NCE): 30, fixed first mass 200

m/z). The isolation scheme consisted of 26 variable windows covering the 350-1,650 *m/z* range with an overlap of 1 *m/z* (100).

DIA data processing and statistical analysis. DIA data was processed in Spectronaut (version 15.6.211220.50606) using directDIA. Data extraction parameters were set as dynamic and non-linear iRT calibration with precision iRT was selected. Data was searched against the *Mus musculus* reference proteome with 58,430 entries (UniProtKB-TrEMBL), accessed on 01/31/2018. Trypsin/P was set as the digestion enzyme and two missed cleavages were allowed. Cysteine carbamidomethylation was set as a fixed modification; methionine oxidation and protein N-terminus acetylation were set as dynamic modifications. Identification was performed using 1% precursor and protein q-value. Quantification was based on the peak areas of extracted ion chromatograms (XICs) of 3 – 6 MS2 fragment ions, specifically b- and y-ions, with local normalization and q-value sparse data filtering applied (Supplemental Table S4). In addition, iRT profiling was selected. Senescence specific differential protein secretion analysis comparing samples derived from unirradiated and senescent *M. musculus* and *M. spretus* cells was performed using the proteomics data as input for a two-factor ANOVA with Benjamini-Hochberg multiple testing correction (102). Only those proteins with a corrected *p*-value < 0.05 were considered significantly differentially secreted between the species during senescence.

Transcriptomic screen for senescence regulators

To associate expression variation in genes with sequence variation in their upstream binding sites for a given transcription factor, we proceeded as follows. From RNA-seq profiling of *M. musculus* x *M. spretus* F1 hybrid cells (see above), we used the TPM counts for each parent species' allele from each replicate profile from control and senescent conditions as input into a

two-factor ANOVA. A given gene was categorized as exhibiting senescence-associated differential allele specific expression if the interaction F statistic value from this ANOVA was among the top 25% of all genes tested. Separately, we used compiled data from chromatin immunoprecipitation via high-throughput sequencing from the Gene Transcription Regulation Database (GTRD) (34) to identify all experimentally determined transcription factor (TF) binding sites located within a 5kb window upstream of the transcriptional start site for each gene in turn in the *M. musculus* genome; we refer to the downstream gene of each such binding location as the target of the TF. This calculation used *M. musculus* gene start sites from the Ensembl GRCm38.96 GFF. Next, for each binding site, we used the VCF between PWK and STF pseudogenomes (see above) to identify single nucleotide variants between PWK and STF in the binding site locus. Now, for all the target genes of a given TF, we categorized them as having sequence variants or not in the respective binding site, and exhibiting senescence-associated differential allele-specific expression. We eliminated from further consideration any TF with fewer than 250 target genes in each of the four categories. For all remaining TFs, the 2 x 2 contingency table was used as input into a Fisher's exact test with Benjamini-Hochberg multiple testing correction.

Usf2 shRNA vector design, construction and application

Usf2 knockdown shRNA sequences were obtained from the Broad Institute Genetic Perturbation Portal (https://portals.broadinstitute.org/gpp/public/). Two shRNA sequences for *Usf2* (CCGGGCAAGACAGGAGCAAGTAAAGCTCGAGCTTTACTTGCTCCTGTCTTGCTTTTTTGAAT; CCGGACAAGGAGACATAATGCATTTCTCGAG-AAATGCATTATGTCTCCTTGTTTTTTTGAAT), and, separately, a scrambled control sequence (CCTAAGGTTAAGTCGCCCTCGCTCGAGCGAGGGCGACTTAACCTTAGG, Addgene cat.

#1864), were each cloned into pLKO.1 puro lentiviral vectors (Addgene cat. #8453). Lentiviral particles containing each of the shRNA constructs were generated by calcium phosphate co-transfection of HEK 293T cells with the shRNA pLKO.1 puro vectors and separate pMDLg/pRRE packaging and pCMV-VSV-G envelope plasmids generously provided by Dr. Marius Walter of the Verdin Lab at the Buck Institute. The number of viral particles generated was determined using the Origene One-Wash™ Lentivirus Titer Kit, p24 ELISA (cat. #TR30038). These particles were used to infect two biological replicates of purebred *M. musculus* (PWK) primary tail fibroblasts at a multiplicity of infection of 5 with 4 µg/mL of polybrene, and infected cells were selected by incubating with 2 µg/mL puromycin for 10 days, changing media and antibiotic every other day. Knockdown of *Usf2* was determined by qPCR, using *Usf2* qPCR primer sequences chosen through NCBI Primer Blast, filtering for those spanning an exon-exon junction. The primer pair with the same efficiency (calculated as $10^{(-1/slope)}$ when plotting log concentration of template cDNA versus Ct) as the internal control *Actb* qPCR primers was chosen: *Usf2* forward 5' TTCGGCGACCACAATATCCAG 3', *Usf2* reverse 5' TTCGGCGACCACAATATCCAG 3', *Actb* forward 5' CAACCGTGAAAAGATGACCC 3', *Actb* reverse 5' GTAGATGGGCACAGTGTGGG 3'. *Usf2* expression was calculated using the Delta-Delta Ct method (103).

Cell proliferation and DNA damage assays

For each of two biological replicates of purebred *M. musculus* (PWK) cells infected with lentivirus harboring the scrambled control and two of each *Usf2* knockdown, either before irradiation or 6 hours after irradiation (see above), we measured cell proliferation and DNA damage response as follows.

For a given replicate, DNA synthesis was measured via 5-ethynyl-2´-deoxyuridine (EdU) incorporation assays using the Invitrogen™ Click-iT™ Edu Alexa Fluor™ 488 Flow Cytometry Assay Kit (cat. #C10420). Cells were treated with 5 µM EdU in complete medium and left in the incubator overnight. The following day cells were fixed, permeabilized, and treated with Alexa Fluor™ 488 azide before running through a BD LSRFortessa™ Cell Analyzer to identify the percentage of EdU positive cells.

For a given replicate, we carried out a comet assay to measure levels of DNA double stranded breaks for a given replicate culture as described (53). Briefly, slides scored with a diamond tipped scribe were dipped in 1% low melting point agarose and left at 4ºC overnight. Cells of all genotypes tested were mixed into 1% low melting point agarose at 2×10^4 cells/ml, spread over the prepared slides and left to solidify for 1 hour. Slides were then incubated at 37ºC in 2% sarkosyl, 0.5 M NA_2EDTA and 0.5 mg/mL proteinase K pH 8 lysis buffer overnight. The following day the slides were washed three times in 90 mM Tris, 90 mM boric acid, and 2 mM NA_2EDTA pH 8.5 wash buffer, then subject to electrophoresis at 0.6 V/cm for 25 minutes in wash buffer. The slides were then washed three times in distilled water and placed in a staining solution containing 5 µg/mL of propidium iodide for 20 minutes. The slides were washed again once with distilled water and multiple representative images were taken of each sample using a Zeiss AxioObserver epi-fluorescent microscope. Images were processed via ZEN Digital Imaging for Light Microscopy (RRID:SCR_013672) and comet tail moments were analyzed via OpenComet (104) in ImageJ (105).

For H2AX assays, for a given replicate, cells were cultured in 8-chamber Nunc™ Lab-Tek™ II Chamber Slides™ (Thermo Fisher cat. # 154453). The day before staining, all cells were seeded at 60-70% confluence in each chamber. Cells were fixed by incubating with 4% paraformaldehyde for 5 minutes at 4ºC and permeabilized using 0.1% Triton X-100 for 15

minutes at room temperature. The cells were then blocked using 3% bovine serum albumin (BSA) in PBS for 45 minutes at room temperature, then incubated with 1 µg/mL of primary antibodies specific to phosphorylated (Ser 139) H2AX (cat. # sc-517348, Santa Cruz Biotechnology) in 3% BSA overnight at 4ºC. The following day the cells were washed in PBS three times before incubating with 2 µg/mL of Alexa 488 secondary antibodies purchased from Invitrogen (cat. # A11001) for two hours at room temperature. Cells were washed three times with PBS then incubated with 0.5 µg/mL DAPI for 5 minutes at room temperature. The cells were washed once more with PBS before mounting for imaging. Multiple representative confocal images of each sample were taken using a Zeiss LSM 710 AxioObserver. Images were processed using ImageJ, taking the average background fluorescence across several nuclei in each field of vision and only counting foci with fluorescence intensities above the background threshold.

In addition to the above, we also carried out EdU incorporation assays on two biological replicates of wild-type primary fibroblasts of the *M. musculus* (PWK) background at five days after irradiation, and observed 0.5 and 1% EdU staining, respectively.

Multivariate ANOVA of irradiation and senescence timecourse

To identify genes whose expression changed in wild-type cells through irradiation and senescence, we used RNA-seq profiling data from purebred *M. musculus* (PWK) cells harboring a scrambled shRNA before and 6 hours, 10 days, and 20 days after irradiation (see Supplemental Table S6) as input into a multivariate ANOVA test.

MERLIN regulatory network reconstruction

To reconstruct a regulatory network we used RNA-seq profiling data for purebred *M. musculus* (PWK) cells harboring a scrambled shRNA or a *Usf2*-targeting RNA, before and 6 hours, 10 days and 20 days after irradiation, as input into MERLIN (106) with default settings. Analysis used a catalog of murine transcription factors from the Gene Transcription Regulation Database (34).

Data access

All raw and processed sequencing data generated in this study have been submitted to the NCBI Gene Expression Omnibus (GEO; https://www.ncbi.nlm.nih.gov/geo/) under accession number GSE201217. Raw data and complete MS data sets have been uploaded to the Mass Spectrometry Interactive Virtual Environment (MassIVE) repository, developed by the Center for Computational Mass Spectrometry at the University of California San Diego, and can be downloaded using the following link: http://massive.ucsd.edu/ProteoSAFe/status.jsp?task=5e7aa6a2b31f4dcfafa679e9d3f3d9c3 (MassIVE ID number: MSV000089246; ProteomeXchange ID: PXD033182). *Enter the username and password in the upper right corner of the page:* Username: MSV000089246_reviewer, Password: winter.

Conflict of interest statement

The authors report no conflicts of interest.

Acknowledgements

The authors thank Mary West for support of cell culture resources, Melissa Chao for help with data collection, and Herbert Kasler, Marius Walter, and Eric Verdin for helpful discussions and materials. This work was supported by National Institutes of Health R01 NS116992 and R01 GM120430 to R.B.B and R01 HD094787 to J.M.G. E.E.K.K. was supported by the National Science Foundation Graduate Research Fellowship Program (DGE-1313190). Any opinions, findings, and conclusions or recommendations expressed in this material are those of the author(s) and do not necessarily reflect the views of the National Science Foundation or the National Institutes of Health.

Author contributions

RBB and TK conceived of the idea of the study; TK carried out fibroblast harvest and culture, RNA-seq, knockdown, and cell-biological assays and all data analysis. BS and CDK carried out proteomics profiling. EEKK, ECM, and JMG carried out all mouse mating and husbandry. TK, JC, and RBB wrote the manuscript with input from all authors.

Figure captions

Figure 1: Senescent *M. spretus* cells exhibit lower β-galactosidase activity. (A) Representative images of senescent primary fibroblasts from *M. musculus* (above) and *M. spretus* (below) stained with the β-galactosidase indicator X-Gal seven days after irradiation. (B) Each trace reports results from a timecourse of X-Gal staining assays of primary senescent cells of the indicated species as in (A). The *y*-axis reports the proportion of cells stained positive for senescence-associated β-galactosidase (SABG) activity. In a given column, small points report biological and technical replicates and large points report their average (*M. musculus* $n = 9$, *M. spretus* $n = 5$). ***, $p < 0.001$, ****, $p < 0.0001$, one-tailed Wilcoxon test comparing species.

Figure 2: Senescent *M. spretus* cells express fewer secreted factors. (A) Each trace reports a cumulative distribution of the change, in senescent primary fibroblasts of the indicated species, in mRNA levels of genes of the senescence associated secretory phenotype (4) with senescence. The *y*-axis reports the proportion of genes with the expression change on the *x*-axis, with the latter taken as an average across replicates. (B) Each row shows results from a test of the genes of the indicated Gene Ontology term for enrichment of expression change between the species during senescence, with *p*-values from a resampling-based test, corrected for multiple testing. (C) Annotations are as in (A) except that measurements were of secreted peptides, and the complete set of peptides with significant differential abundance between species is shown.

Figure 3: A screen correlating divergence in transcription factor binding sites and *cis*-regulatory expression during senescence reveals USF2 as a top hit. (A) *M. musculus* (blue) and *M. spretus* (red) alleles of a gene are expressed differently in interspecific F1 hybrid cells in a senescence-dependent manner, as a product of a sequence variant (green striped) in the binding site for a transcription factor (yellow). (B) Each row reports the multiple testing-corrected *p*-value from a Fisher's Exact Test of target genes of the indicated transcription factor, quantifying association between species differences in experimentally determined binding sites (34) and allele-specific expression in primary cells of the *M. musculus* x *M. spretus* F1 hybrid background before and after senescence induction. Results for all tested factors are listed in Supplemental Table S5. (C) Shown are the input data for the Fisher's Exact Test in (B) for USF2. Each bar reports analysis of genes with USF2 binding sites in their upstream regions that do (right) or do not (left) harbor sequence variants between *M. musculus* and *M. spretus*. For a given bar, genes are categorized by the presence or absence of senescence-dependent differential allele-specific expression (Δ ASE). (D) For each trace, the *x*-axis reports the number of sequence variants between *M. musculus* and *M. spretus* in a given USF2 binding site, and the *y*-axis reports the proportion of all USF2 target genes bearing the number of variants on the *x*, as a kernel density estimate. Colors denote the presence or absence of senescence-dependent differential allele-specific expression at USF2 target genes as in (C). (E) Data are as in (D) except that the *x*-axis reports the distance of the variant from the center of the USF2 binding site.

Figure 4: *Usf2* depletion results in more DNA damage but a muted DNA damage response following irradiation. (A) *M. musculus* primary fibroblasts were infected with a lentivirus encoding a short hairpin RNA (shRNA, SH) targeting *Usf2* or a scrambled control, and analyzed before (SH unirradiated) or six hours after (SH→IR) treatment with ionizing radiation. (B) In a

given row, the second column reports the average, across genes of the indicated Gene Ontology term, of the $\log_2$ of the ratio of expression between cells bearing shRNAs targeting *Usf2* and those with a scrambled control (SCR), six hours after irradiation. The third column reports significance in a resampling-based test for enrichment of directional differential expression between *Usf2* knockdown cells and the scrambled control in the respective term, corrected for multiple testing. The fourth column reports the direction of the change in expression before and six hours after irradiation in cells of the scrambled control genotype. (C) Each trace reports a cumulative distribution of the $\log_2$ of the ratio of expression between cells harboring bearing shRNAs targeting *Usf2* or the scrambled control in genes annotated in apoptosis, before or six hours after irradiation treatment as indicated. The *y*-axis reports the proportion of genes with the expression change on the *x*-axis. (D) Data are as in (C), except that EGFR signaling pathway genes were analyzed. (E) Each column reports tail moments detected in a comet assay on primary fibroblasts harboring the indicated shRNAs, before or six hours after irradiation as indicated. In a given column, points report biological and technical replicates and the bar height reports their average (SCR $n = 5$, *Usf2* KD $n = 20$). ****, $p < 0.0001$, one-tailed Wilcoxon test. (F) Left, each column reports number of γH2AX foci per cell detected in primary fibroblasts harboring the indicated shRNAs six hours after irradiation. In a given column, points report biological and technical replicates and the bar height reports their average (SCR $n = 12$, *Usf2* KD $n = 28$). ***, $p < 0.001$, one-tailed Wilcoxon test. Right, representative images of the indicated cultures.

Figure 5: *Usf2* knockdown results in an enhanced senescence profile. (A) *M. musculus* primary fibroblasts were infected with a lentivirus encoding an shRNA (SH) targeting *Usf2* or a scrambled control, and analyzed before (SH unirradiated) or after (SH→SEN) treatment with ionizing radiation (IR) to induce senescence (SEN). (B) Data are as in Figure 4B except that

cells were analyzed 10 days after irradiation. (C) *M. musculus* primary fibroblasts were irradiated, incubated for 10 days to senesce, then infected with shRNAs and analyzed after 10 additional days. (D) Data are as in (B) except that cells from the scheme in (C) were analyzed. (E) Each trace reports a cumulative distribution of the $\log_2$ of the ratio of expression in cells bearing shRNAs targeting *Usf2* and those with a scrambled control (SCR), in genes annotated in the inflammatory response, when shRNAs were administered to a resting culture (SH unirradiated), to resting cells followed by irradiation (SH→SEN), or after irradiation and senescence establishment (SEN→SH). The *y*-axis reports the proportion of genes with the expression change on the *x*-axis, with the latter taken as an average across replicates. (F) Data are as in (E), except that genes involved in G2/M transition of mitotic cell cycle were analyzed. (G) Left, each column reports the proportion of senescence associated β-galactosidase (SABG) positive cells treated with the indicated shRNAs in resting culture (unirradiated) or 7 days after irradiation (SEN). In a given column, points report biological and technical replicates and the bar height reports their average (unirradiated $n = 4$, SEN $n = 24$). **, $p < 0.01$, one-tailed Wilcoxon test. Right, representative images of the indicated cultures.

Supplemental figure captions

Supplemental Figure S1: Senescent *M. spretus* primary fibroblasts display muted mRNA induction of genes of the senescence-associated secretory phenotype. Each column reports expression (TPM, transcripts per million) from RNA-seq profiling of primary fibroblasts from the indicated species for the indicated genes, in control or irradiation-induced senescent (SEN) cells. In a given column, points report biological replicates and the bar height reports their average (n = 3).

Supplemental Figure S2: Senescent *M. spretus* primary fibroblasts display muted secretion of proteins of the senescence-associated secretory phenotype. Data are as in Supplemental Figure S1 except that protein abundance from conditioned medium is shown.

Supplemental Figure S3: Senescent *M. musculus* x *M. spretus* F1 primary fibroblasts display intermediate activity of senescence-associated β-galactosidase (SABG). Each column reports the proportion of SABG positive cells for the indicated genotype in control cells or in senescent cells seven days after irradiation (SEN). In a given column, points report biological and technical replicates and the bar height reports their average (*M. musculus* n = 9, *M. spretus* n = 5, F1 hybrid n = 2).

Supplemental Figure S4: Variation in gene expression during senescence between *M. musculus* and *M. spretus* is controlled by both *cis*- and *trans*-acting elements. Each point represents expression of one gene in primary fibroblasts induced to senesce. The x-axis reports the ratio of expression, as an average across biological replicates, measured in purebred *M. musculus* (Mm) and *M. spretus* (Ms) cells; the y-axis reports the ratio of allele-

specific expression from the *M. musculus* and *M. spretus* alleles in cells from the interspecific F1 hybrid.

Supplemental Figure S5: Senescent *M. musculus* x *M. spretus* F1 primary cells display intermediate induction in mRNA expression of genes of the senescence-associated secretory phenotype. Data are as in Figure 2A of the main text except that measurements from the interspecific F1 hybrid are shown in green.

Supplemental Figure S6: *Usf2*-targeting shRNAs knock down *Usf2* expression. Each set of bars reports *Usf2* expression measured via qPCR in *M. musculus* primary cells, in one biological replicate. In a given replicate, each bar reports the fold change (FC) in *Usf2* expression between cells harboring *Usf2*-targeting shRNA (*Usf2* KD) and those with a scrambled shRNA (SCR), normalized with respect to the value of the latter.

Supplemental Figure S7: *Usf2* depletion slightly slows growth of primary *M. musculus* cells independent of irradiation. Each column reports the percentage of EdU incorporation in primary fibroblasts harboring *Usf2* or scrambled shRNAs, before or six hours after irradiation as indicated. *, $p < 0.05$, one-tailed Wilcoxon test. In a given column, points report biological and technical replicates and the bar height reports their average (SCR $n = 11$, *Usf2* KD $n = 22$).

Supplemental Figure S8: *Usf2* knockdown results in less transcriptional repression following acute DNA damage. In a given panel, each column reports mRNA expression of the indicated gene in transcripts per million (TPM) in primary fibroblasts harboring *Usf2* or scrambled shRNAs, before or six hours after irradiation as indicated. (A) Shown are a representative subset of the genes that were repressed in cells harboring the scrambled shRNA control following acute DNA damage. (B) Shown are genes in the Gene Ontology term

"epidermal growth factor receptor signaling pathway." Inset reports genes with average TPM >125 in one or more samples. In a given column, points report biological replicates and the bar height reports their average (*n* = 3).

Supplemental Figure S9: Expression of core DNA damage response genes are largely not affected by *Usf2* knockdown. Data are as in Supplemental Figure S8 except that DNA damage response genes are shown.

Supplemental Figure S10: *Usf2* knockdown results in an enhanced senescent gene expression profile. In a given panel, each column reports mRNA expression in transcripts per million (TPM) in primary fibroblasts harboring *Usf2* or scrambled shRNAs, when shRNAs were administered to a resting culture (unirradiated), to resting cells followed by irradiation (→SEN), or after irradiation and senescence establishment (→KD). (A) Genes annotated in inflammation and immune response that were upregulated during senescence in scrambled shRNA controls. (B) Genes annotated in cell cycle that were repressed with senescence in scrambled shRNA controls. In a given column, points report biological replicates and the bar height reports their average (SCR *n* = 2, *Usf2* KD *n* = 4).

Supplemental Figure S11: Expression profiling of control cells during a senescence timecourse reveals a dynamic expression program with senescence progression. Each trace reports a cumulative distribution of gene expression in primary *M. musculus* fibroblasts harboring a scrambled shRNA, at the indicated timepoint after irradiation treatment relative to unirradiated controls. Included in the distribution are all genes significant in a test for significant expression change across the timepoints by multivariate ANOVA (Supplemental Table S10). The *y*-axis reports the proportion of genes with the expression change on the *x*-axis.

Supplemental table captions

Supplemental Table S1: RNA-seq gene expression profiling of resting and senescent purebred *M. musculus* and *M. spretus* primary cells. Each row reports expression of the indicated gene in transcripts per million, as an average across biological replicates of primary fibroblasts from the indicated background cultured in the indicated condition. Columns report expression in purebred *M. musculus* (Mm) or *M. spretus* (Ms) primary fibroblasts, or expression from each allele (*M. musculus*, Mm; *M. spretus*, Ms) in primary fibroblasts from the interspecific F1 hybrid, in unirradiated control (CONT) or 10 days after irradiation (senescent, SEN).

Supplemental Table S2: Functional-genomic enrichment analysis of expression profiles of unirradiated purebred *M. musculus* and *M. spretus* primary cells. Each row reports the results of a resampling test for enrichment of expression change between unirradiated primary fibroblasts from purebred *M. musculus* and *M. spretus* (see Supplemental Table S1) for the indicated Gene Ontology biological process term. The second column represents the absolute value of the sum of the ratios of expression in *M. musculus* versus *M. spretus* for all the genes in the indicated term. The third column reports the number of genes with expression data in the term. The fourth column reports the raw *p*-value from resampling analysis, and the final column reports Benjamini-Hochberg corrected *p*-values. Only terms with significant enrichment (corrected $p < 0.05$) are shown.

Supplemental Table S3: Functional-genomic enrichment analysis of expression profiles of senescent purebred *M. musculus* and *M. spretus* primary cells. Data are as in Supplemental Table S2 except that *M. musculus* and *M. spretus* cells were analyzed 10 days after irradiation (see Supplemental Table S1).

Supplemental Table S4: Proteomic profiling of conditioned medium from purebred *M. musculus* and *M. spretus* primary cells via mass spectrometry. Columns report the abundance of the indicated protein via mass spectrometry, as an average over replicates and individual detected peptides, in conditioned medium from *M. musculus* (Mm) or *M. spretus* (Ms) cells, each as an unirradiated control (CONT) or 10 days after irradiation (senescent, SEN).

Supplemental Table S5: A screen correlating divergence in transcription factor binding sites and *cis*-regulatory expression during senescence. Each row reports the results of a Fisher's exact test relating, for the indicated transcription factor, two measures of variation between *M. musculus* and *M. spretus*: sequence variants at the factor's experimentally determined binding sites (34) upstream of genes, and, at these genes, senescence-specific expression differences between the two species' alleles in fibroblasts of the F1 hybrid background. The second and third columns report nominal and Benjamini-Hochberg corrected *p*-values respectively.

Supplemental Table S6: Expression profiling of shRNA-expressing purebred *M. musculus* primary cells across a timecourse of irradiation and senescence. Columns report expression of the indicated gene in transcripts per million, as an average across biological replicates, in purebred primary fibroblasts from *M. musculus* (PWK) subjected to either of two regimes. In one, cells were first infected with lentivirus expressing the indicated short hairpin RNA (shRNA) and then profiled before (CONT) or 6 hours (6HR) or 10 days (SEN.10d) after irradiation. In the other regime, cells were irradiated, then infected with lentivirus expressing the indicated shRNA, and then profiled 20 days later (SEN.20d). Usf2, *Usf2* targeting shRNA; SCR, scrambled control shRNA.

Supplemental Table S7: Functional-genomic enrichment analysis of shRNA-expressing purebred *M. musculus* primary cells in untreated conditions. Data are as in Supplemental Table S2 except that *M. musculus* (PWK) primary cells harboring short hairpin RNAs targeting *Usf2* or a scrambled control were cultured in unirradiated conditions (see Supplemental Table S6); for each gene we formulated the average expression measurement across replicates from each shRNA category in turn, and we then took the ratio between these averages for input into Gene Ontology enrichment tests.

Supplemental Table S8: Functional-genomic enrichment analysis of purebred *M. musculus* primary cell transcriptomes upon *Usf2* knockdown and irradiation. Data are as in Supplemental Table S7 except that cells were infected with lentivirus expressing the indicated short hairpin RNA (shRNA), treated with ionizing radiation, and profiled 6 hours afterward (see Supplemental Table S6).

Supplemental Table S9: Functional-genomic enrichment analysis of purebred *M. musculus* primary cell transcriptomes upon *Usf2* knockdown, irradiation, and senescence establishment. Data are as in Supplemental Table S7 except that cells were infected with lentivirus expressing the indicated short hairpin RNA (shRNA), treated with ionizing radiation, and profiled 10 days afterward (see Supplemental Table S6).

Supplemental Table S10: Expression analysis of purebred *M. musculus* primary cells across a timecourse of irradiation and senescence. Each row reports results from analysis of expression of one gene in *M. musculus* (PWK) primary cells harboring a scrambled short hairpin RNA, before and 6 hours, 10 days, and 20 days after irradiation (see Supplemental Table S6). Second and third columns report the raw and Benjamini-Hochberg corrected *p*-values respectively from a multivariate ANOVA test for variation in expression across the

timecourse. Only genes with significant differential expression across the timecourse (corrected $p < 0.05$) are shown.

Supplemental Table S11: Functional-genomic enrichment analysis of purebred *M. musculus* primary cell transcriptomes upon irradiation, senescence establishment, *Usf2* knockdown, and long-term senescence. Data are as in Supplemental Table S2 except that *M. musculus* (PWK) primary cells were irradiated, incubated for 10 days, infected with lentivirus harboring short hairpin RNAs targeting *Usf2* or a scrambled control, and allowed to maintain senescence for another 10 days (see Supplemental Table S6); for each gene we formulated the average expression measurement across replicates from each shRNA category in turn, and we then took the ratio between these averages for input into Gene Ontology enrichment tests.

Supplemental Table S12: *In silico* regulatory network reconstruction from irradiation and senescence transcriptomes. Shown are results from regulatory network inference using all shRNA treated transcriptomes in this study (see Supplemental Table S6) as input into the MERLIN package (106). Each row reports results from a transcription factor inferred to be a downstream target of USF2. The second column reports the strength of the inferred regulation by USF2; negative values indicate repression. In the remaining columns, “Yes” indicates that one or more genes of the indicated GO term were inferred to be targets of the indicated factor.

Supplemental Table S13: Mouse metadata. Shown are characteristics of mice used for tail cuttings and fibroblast isolation in this study.

Figure 1

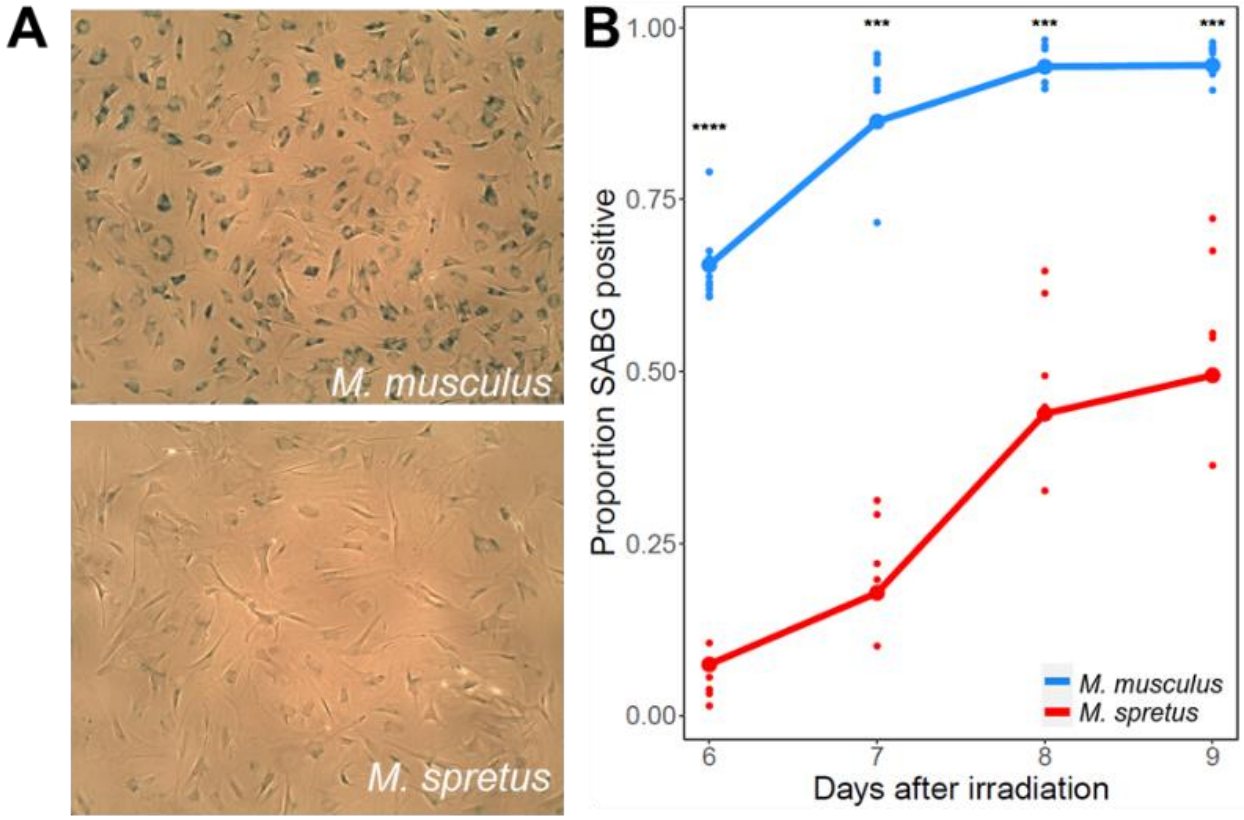
A
M. musculus
M. spretus
B
1.00
0.75
0.50
0.25
0.00
Proportion SABG positive
****
***
***
***
6
7
8
9
Days after irradiation
M. musculus
M. spretus

Figure 2

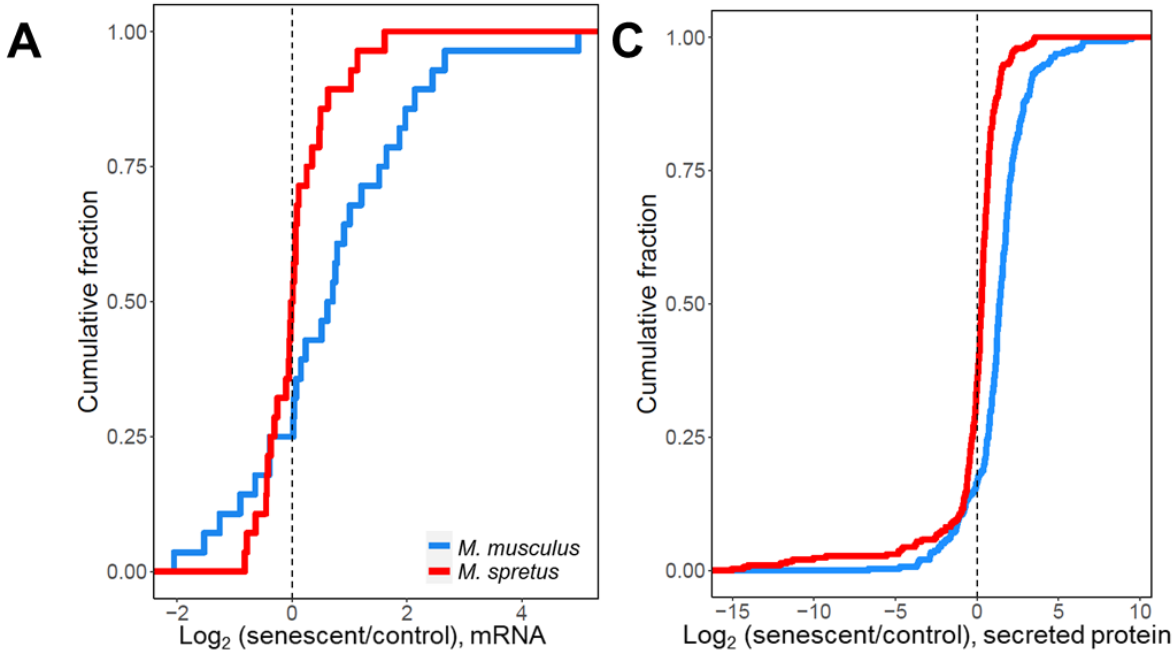

B

GO term	*M. mus* / *M. spr* effect size	p-value	SEN direction in *M. mus* | *M. spr*
antimicrobial humoral immune response mediated by antimicrobial peptide	0.7051633	0.000000	+ | +
regulation of NIK/NF-kappaB signaling	0.3395436	0.000000	+ | -
immune response	0.7865077	0.000000	+ | +
neutrophil chemotaxis	0.4491496	0.018600	+ | +

Figure 3

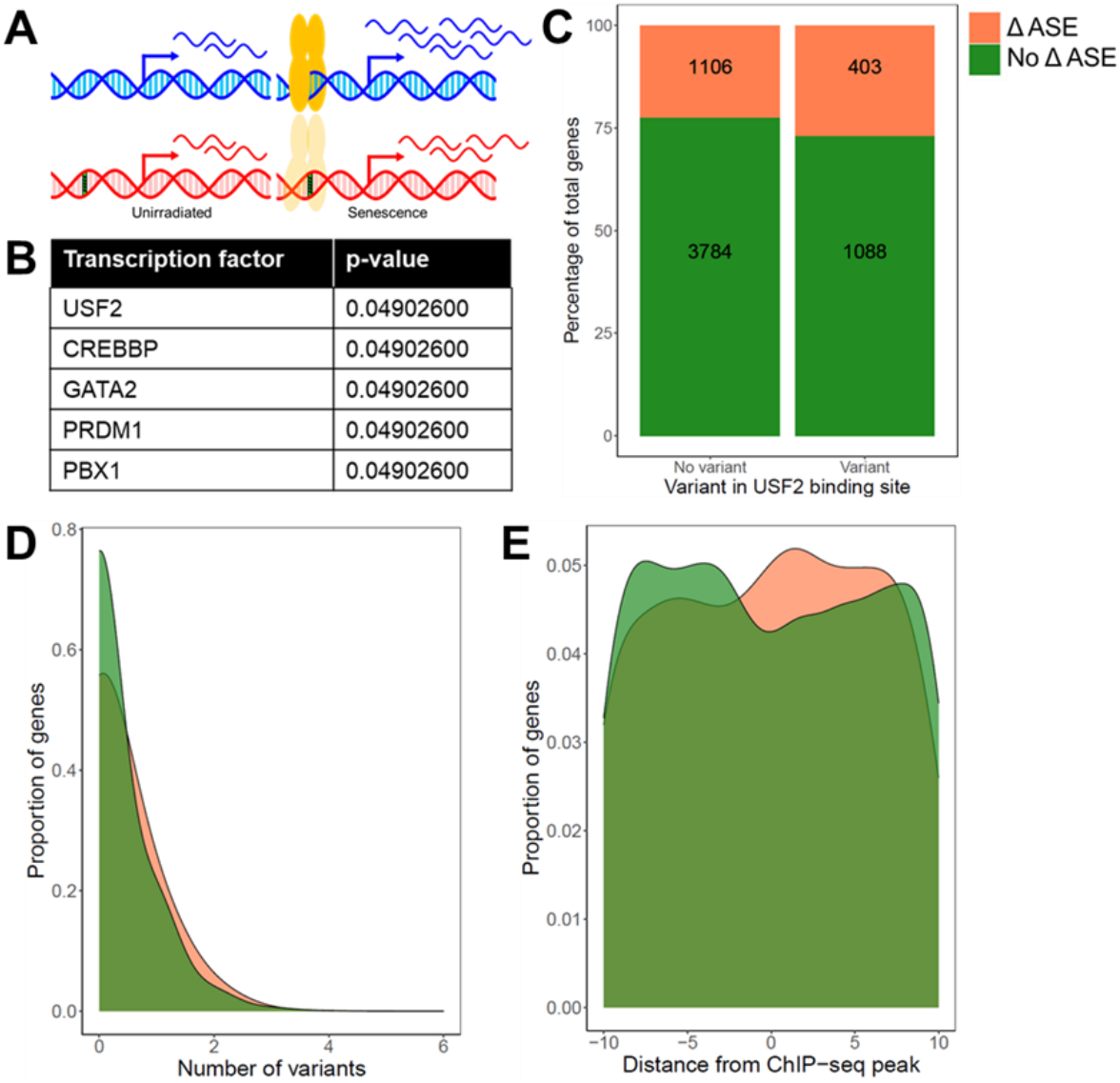

Transcription factor	p-value
USF2	0.04902600
CREBBP	0.04902600
GATA2	0.04902600
PRDM1	0.04902600
PBX1	0.04902600

Figure 4

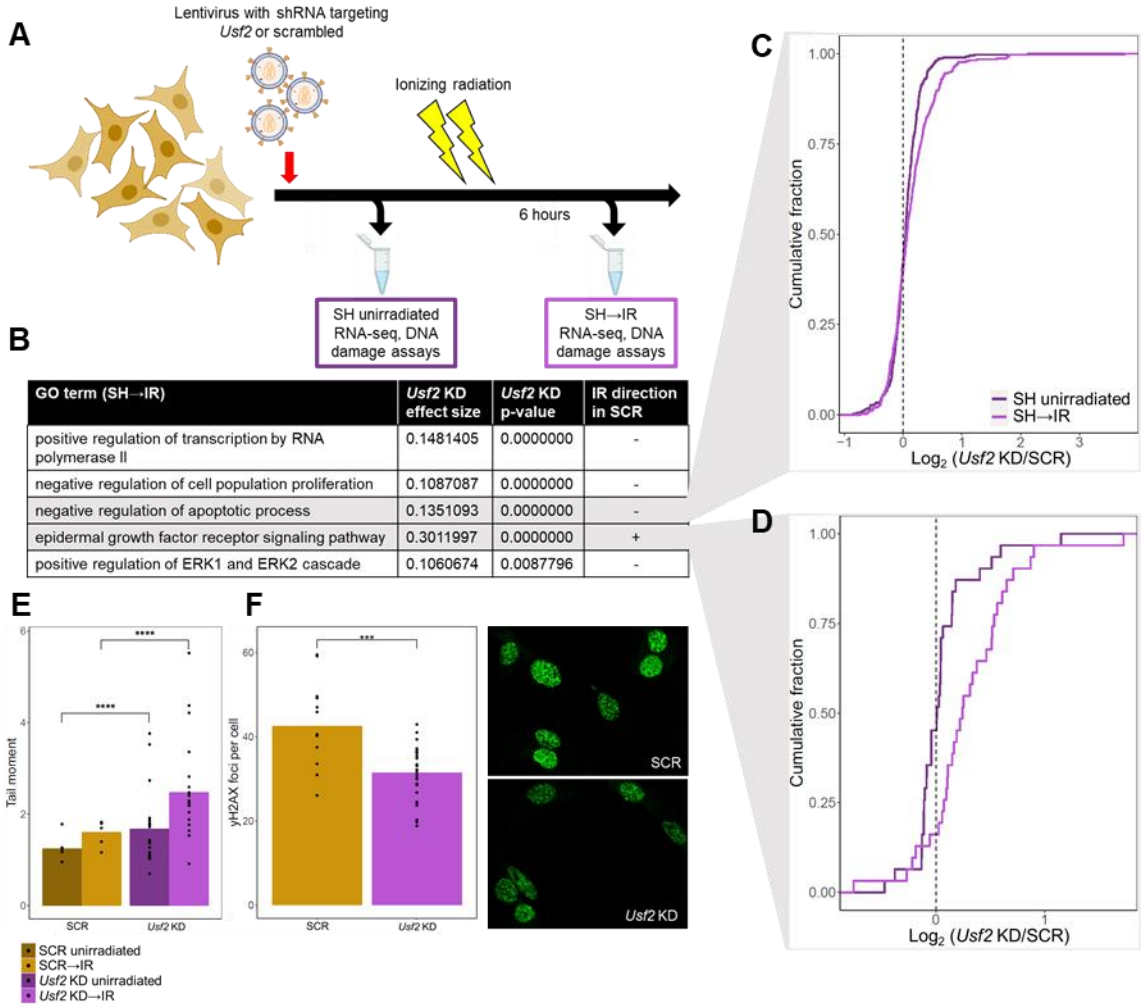

GO term (SH→IR)	*Usf2* KD effect size	*Usf2* KD p-value	IR direction in SCR
positive regulation of transcription by RNA polymerase II	0.1481405	0.0000000	-
negative regulation of cell population proliferation	0.1087087	0.0000000	-
negative regulation of apoptotic process	0.1351093	0.0000000	-
epidermal growth factor receptor signaling pathway	0.3011997	0.0000000	+
positive regulation of ERK1 and ERK2 cascade	0.1060674	0.0087796	-

Figure 5

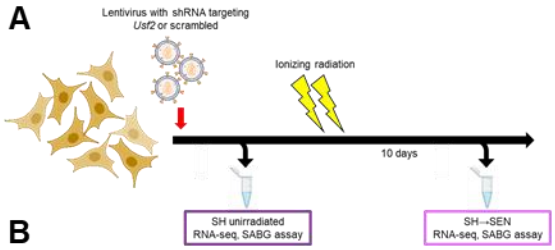

B

GO term (SH→SEN)	*Usf2* KD effect size	*Usf2* KD p-value	SEN direction in SCR
cell cycle	-0.2668974	0.0000000	-
DNA repair	-0.192414	0.0000000	-
positive regulation of interferon-gamma production	0.08790005	0.0075744	+
innate immune response	0.0606095	0.0087758	+
neutrophil chemotaxis	0.1427299	0.0364812	+

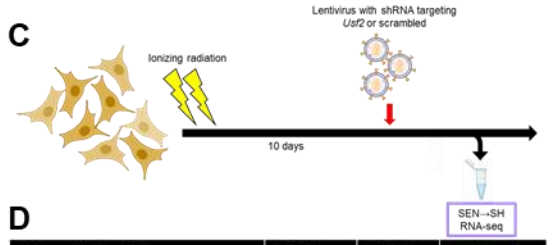

D

GO term (SEN→SH)	*Usf2* KD effect size	*Usf2* KD p-value	SEN direction in SCR
cell cycle	-0.1812952	0.0000000	-
DNA repair	-0.1369582	0.0000000	-
inflammatory response	0.1219121	0.0000000	+
positive regulation of angiogenesis	0.1455308	0.0036357	+
innate immune response	-0.0474851	0.0088779	+
G2/M transition of mitotic cell cycle	-0.2451783	0.0111868	-

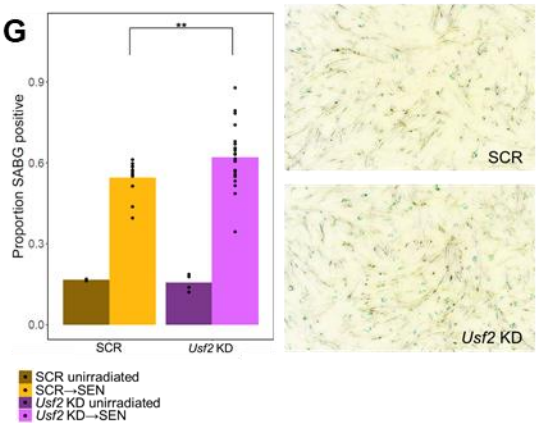

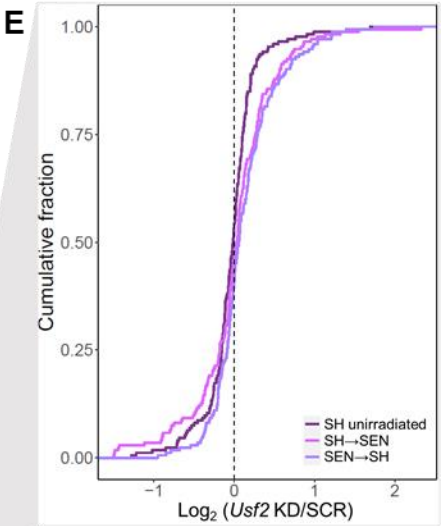

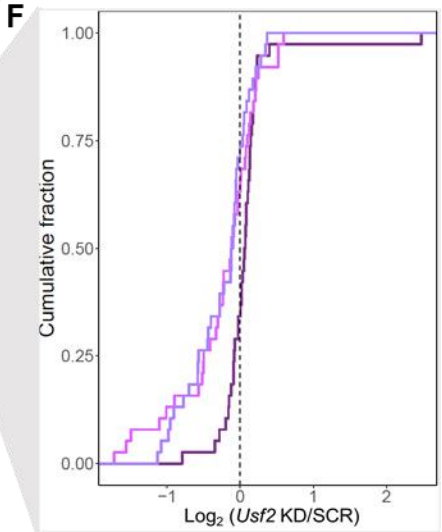

Supplemental Figure S1

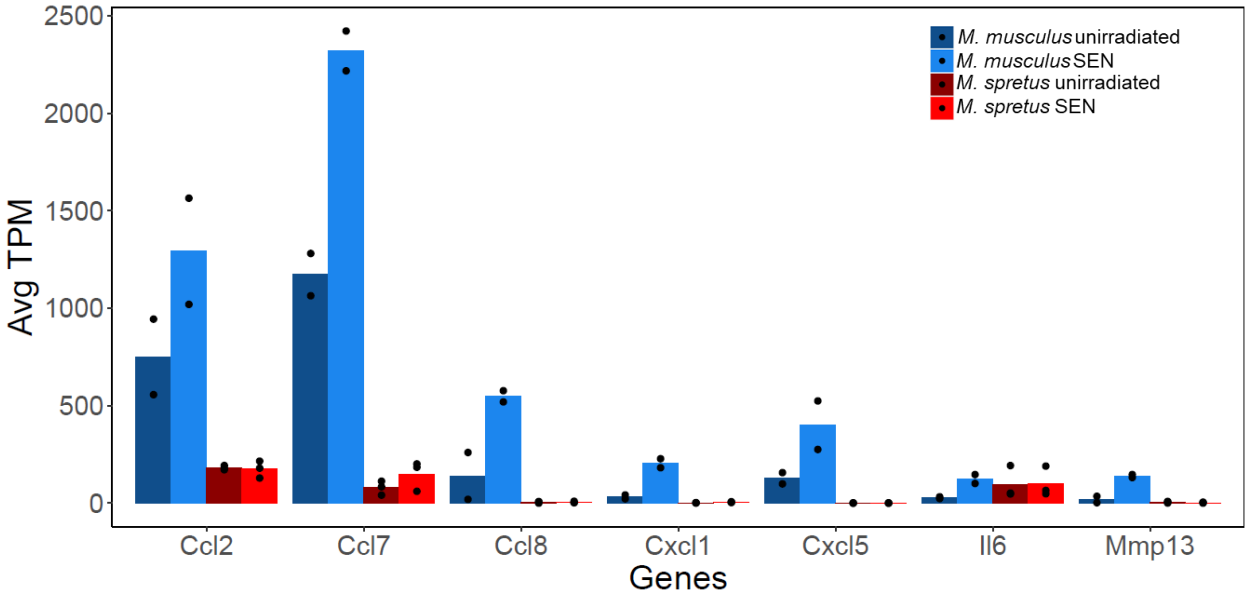

Supplemental Figure S2

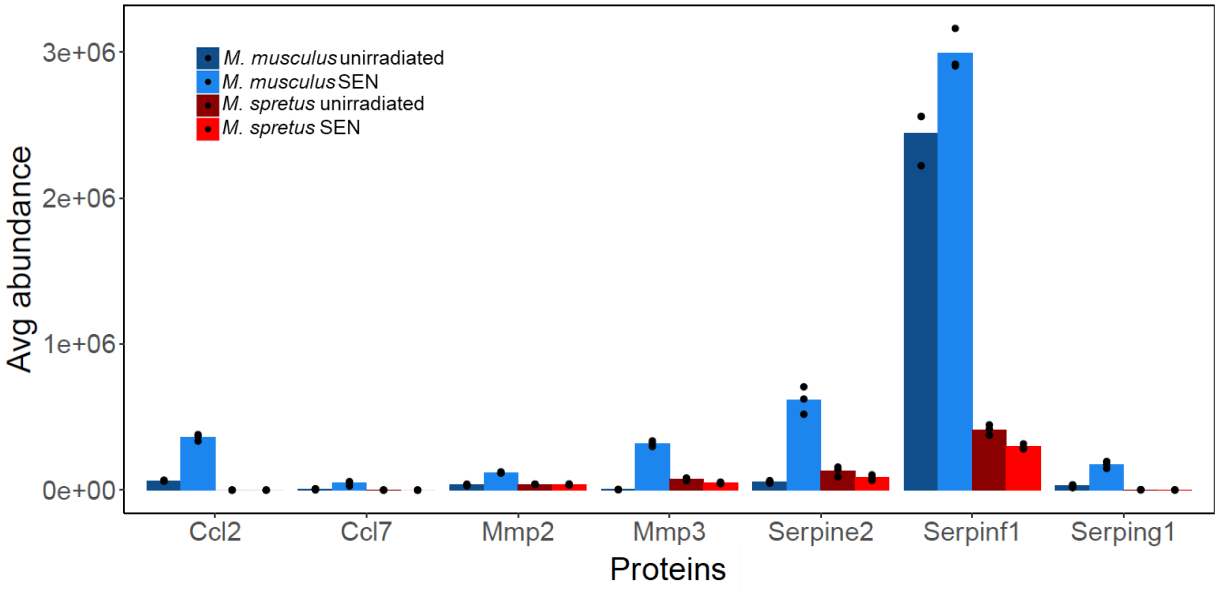

Supplemental Figure S3

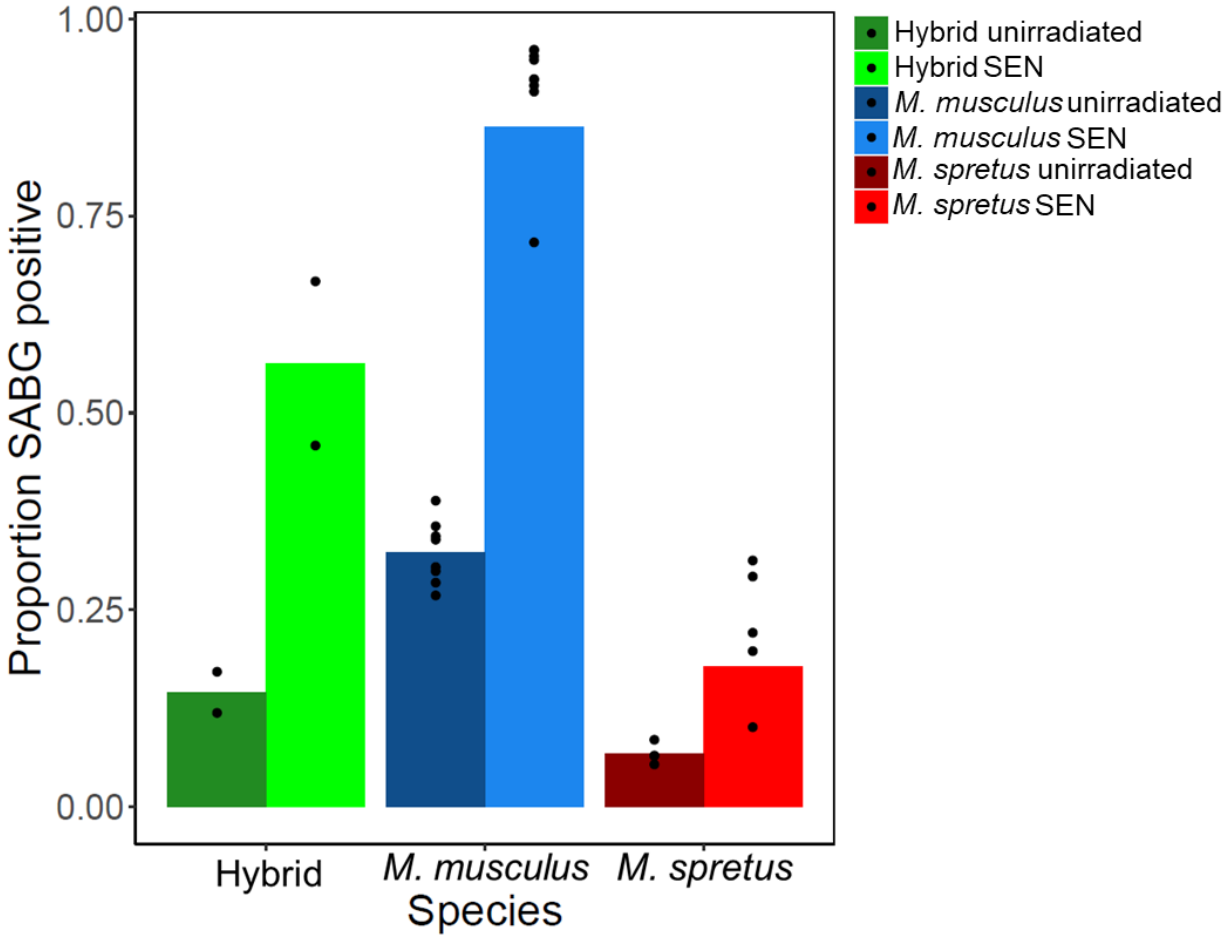

Supplemental Figure S4

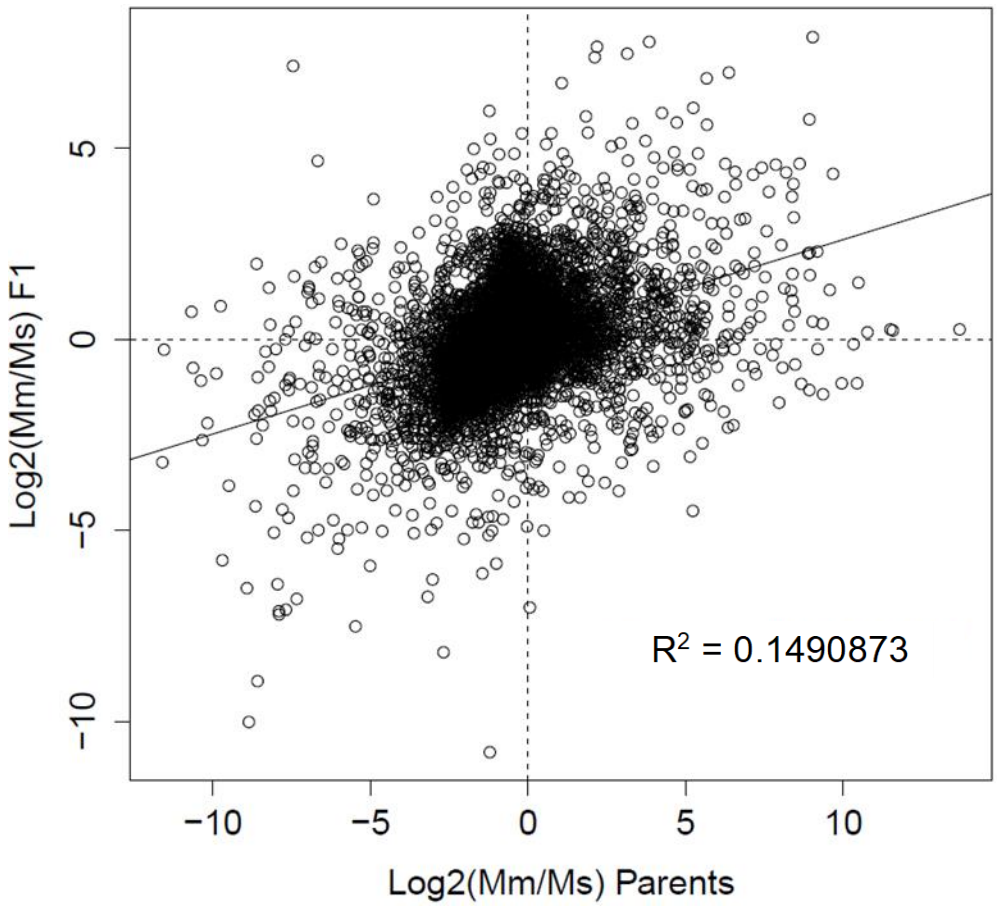

Supplemental Figure S5

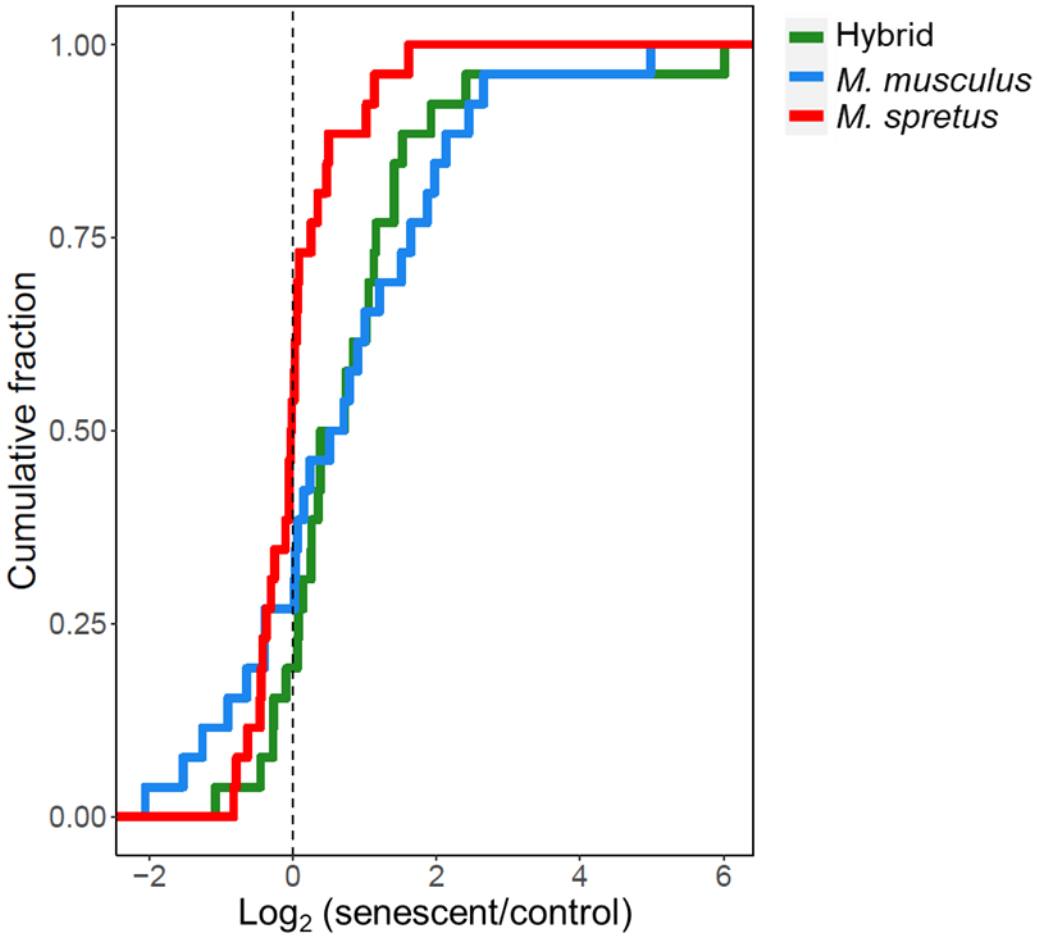

Supplemental Figure S6

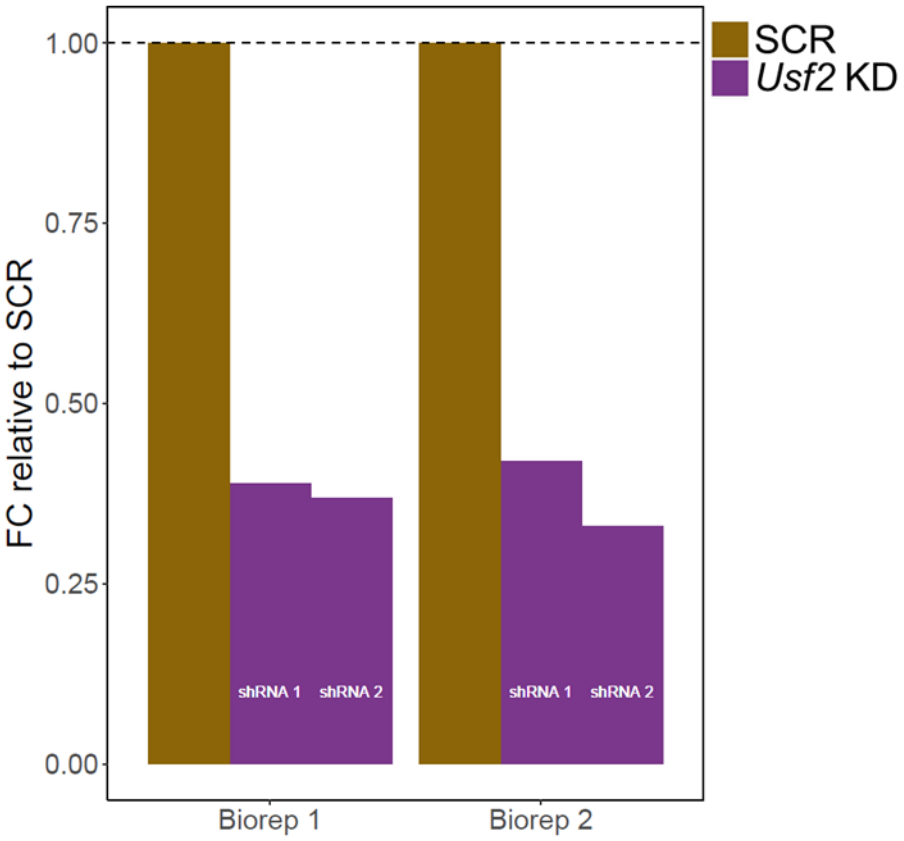

Supplemental Figure S7

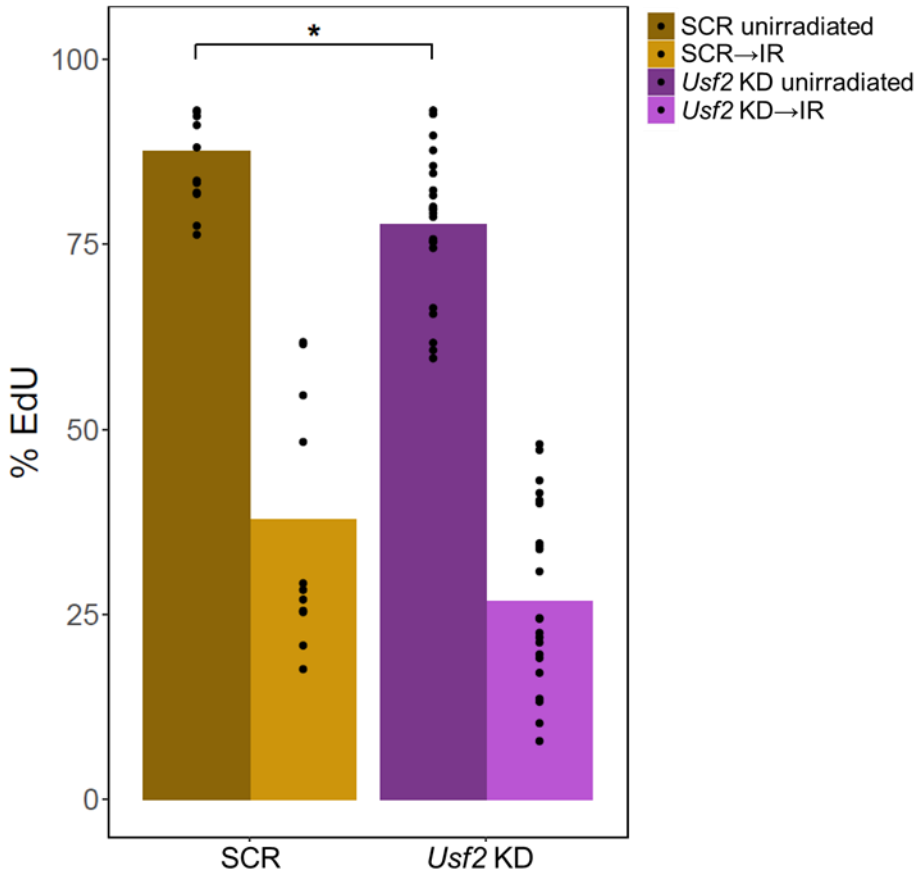

Supplemental Figure S8

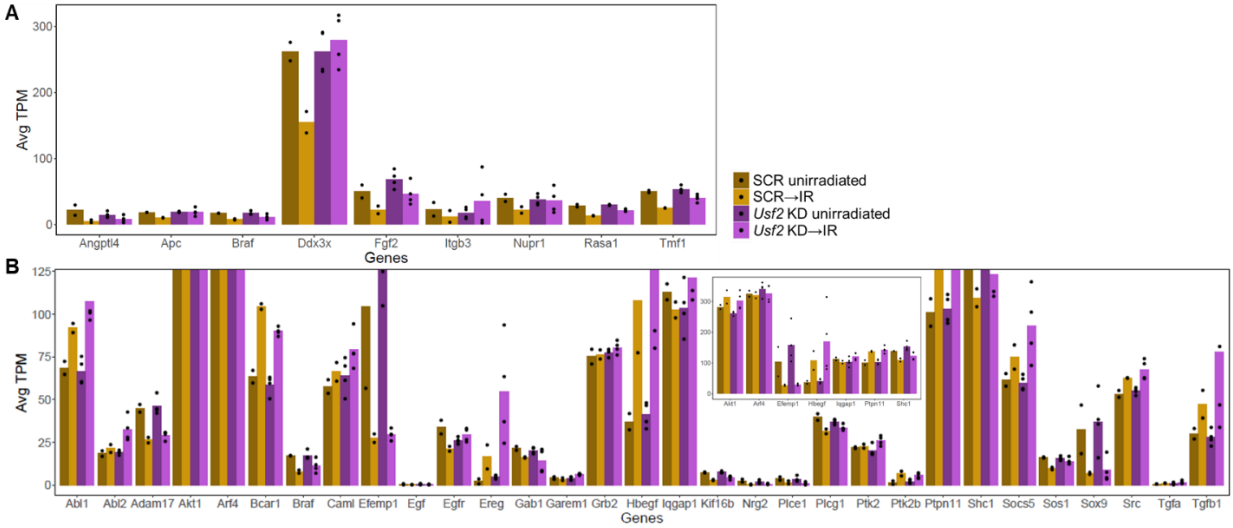

Supplemental Figure S9

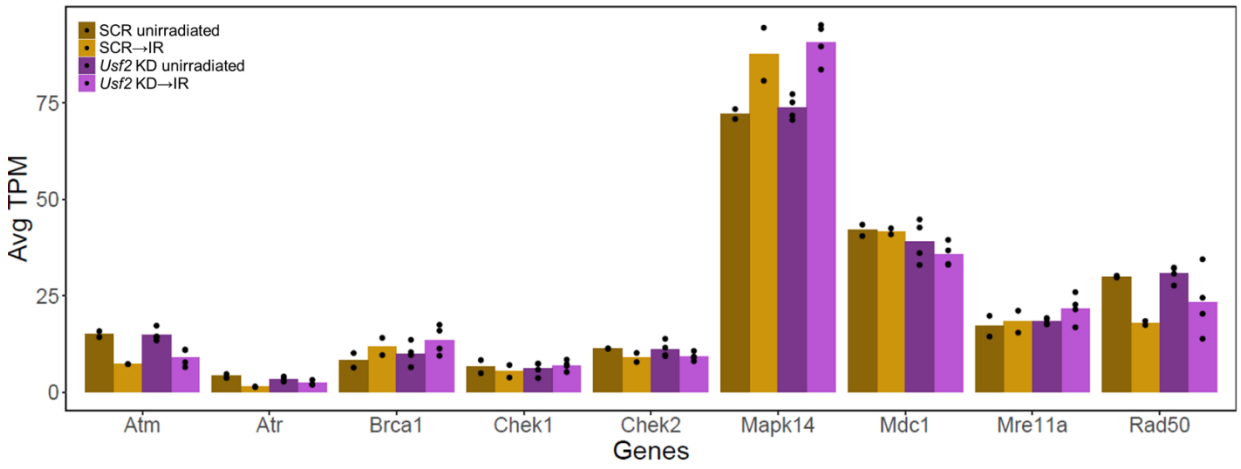

Supplemental Figure S10

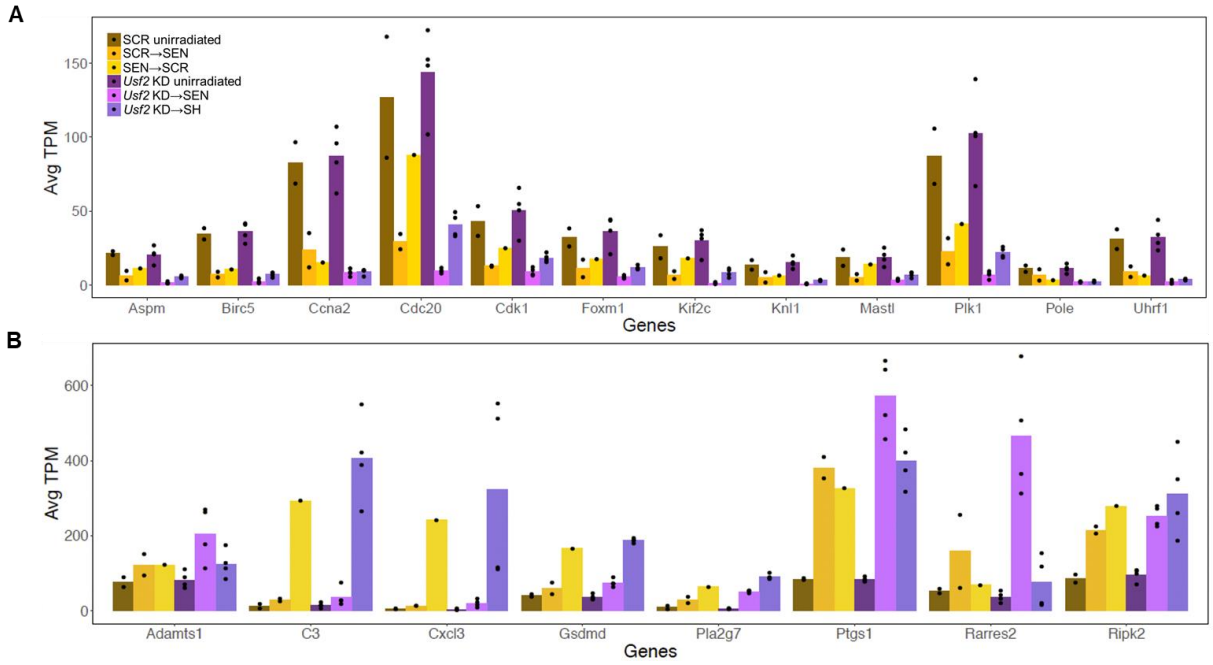

Supplemental Figure S11

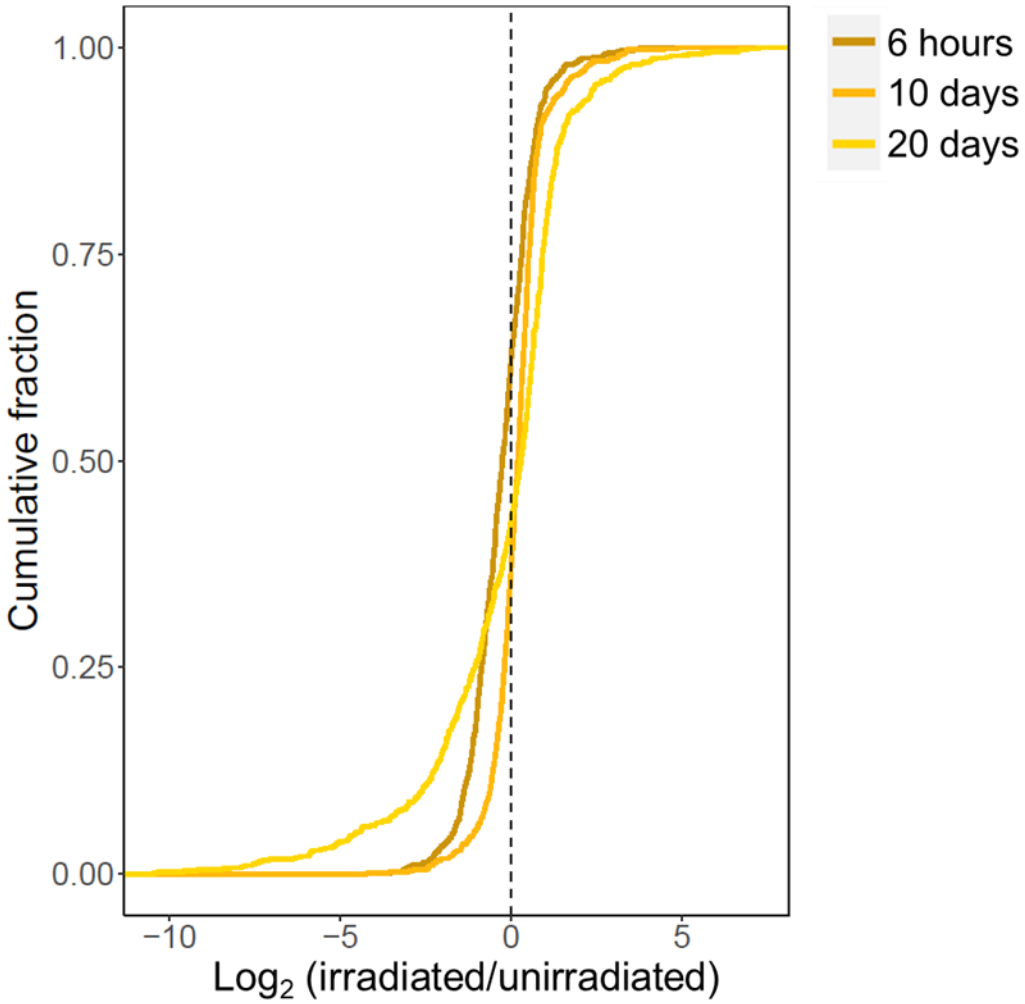

References

1. Hayflick L. The limited in vitro lifetime of human diploid cell strains. Exp Cell Res. 1965 Mar 1;37(3):614–36.

2. Campisi J. Senescent cells, tumor suppression, and organismal aging: good citizens, bad neighbors. Cell. 2005 Feb 25;120(4):513–22.

3. Campisi J, Fagagna FDD. Cellular senescence: when bad things happen to good cells. Nat Rev Mol Cell Biol. 2007;

4. Coppé JP, Patil CK, Rodier F, Sun Y, Muñoz DP, Goldstein J, et al. Senescence-Associated Secretory Phenotypes Reveal Cell-Nonautonomous Functions of Oncogenic RAS and the p53 Tumor Suppressor. PLOS Biol. 2008 Dec 2;6(12):e301.

5. Wan M, Gray-Gaillard EF, Elisseeff JH. Cellular senescence in musculoskeletal homeostasis, diseases, and regeneration. Bone Res. 2021 Sep 10;9(1):1–12.

6. Paramos-de-Carvalho D, Jacinto A, Saúde L. The right time for senescence. Bronner ME, editor. eLife. 2021 Nov 10;10:e72449.

7. Baker DJ, Wijshake T, Tchkonia T, LeBrasseur NK, Childs BG, van de Sluis B, et al. Clearance of p16Ink4a-positive senescent cells delays ageing-associated disorders. Nature. 2011 Nov 2;479(7372):232–6.

8. Demaria M, Ohtani N, Youssef SA, Rodier F, Toussaint W, Mitchell JR, et al. An essential role for senescent cells in optimal wound healing through secretion of PDGF-AA. Dev Cell. 2014 Dec 22;31(6):722–33.

9. Olivieri F, Prattichizzo F, Grillari J, Balistreri CR. Cellular Senescence and Inflammaging in Age-Related Diseases. Mediators Inflamm. 2018 Apr 17;2018:e9076485.

10. Davalos AR, Coppe JP, Campisi J, Desprez PY. Senescent cells as a source of inflammatory factors for tumor progression. Cancer Metastasis Rev. 2010 Jun;29(2):273–83.

11. Krtolica A, Parrinello S, Lockett S, Desprez PY, Campisi J. Senescent fibroblasts promote epithelial cell growth and tumorigenesis: a link between cancer and aging. Proc Natl Acad Sci U S A. 2001 Oct 9;98(21):12072–7.

12. Parrinello S, Coppe JP, Krtolica A, Campisi J. Stromal-epithelial interactions in aging and cancer: senescent fibroblasts alter epithelial cell differentiation. J Cell Sci. 2005 Feb 1;118(Pt 3):485–96.

13. Kang C. Senolytics and Senostatics: A Two-Pronged Approach to Target Cellular Senescence for Delaying Aging and Age-Related Diseases. Mol Cells. 2019 Dec;42(12):821–7.

14. Kim EC, Kim JR. Senotherapeutics: emerging strategy for healthy aging and age-related disease. BMB Rep. 2019 Jan;52(1):47–55.

15. Campisi J. Aging, cellular senescence, and cancer. Annu Rev Physiol. 2013;75:685–705.

16. Salotti J, Johnson PF. Regulation of senescence and the SASP by the transcription factor C/EBPβ. Exp Gerontol. 2019 Dec;128:110752.

17. Chan M, Yuan H, Soifer I, Maile TM, Wang RY, Ireland A, et al. Novel insights from a multiomics dissection of the Hayflick limit. eLife [Internet]. 2022 Feb 1 [cited 2022 Mar 10];11. Available from: https://doi.org/10.7554/eLife.70283

18. Wang Y, Xu Q, Sack L, Kang C, Elledge SJ. A gain-of-function senescence bypass screen identifies the homeobox transcription factor DLX2 as a regulator of ATM–p53 signaling. Genes Dev. 2016 Feb 1;30(3):293–306.

19. Xie Q, Peng S, Tao L, Ruan H, Yang Y, Li TM, et al. E2F Transcription Factor 1 Regulates Cellular and Organismal Senescence by Inhibiting Forkhead Box O Transcription Factors. J Biol Chem. 2014 Dec 5;289(49):34205–13.

20. Han R, Li L, Ugalde AP, Tal A, Manber Z, Barbera EP, et al. Functional CRISPR screen identifies AP1-associated enhancer regulating FOXF1 to modulate oncogene-induced senescence. Genome Biol. 2018 Aug 17;19(1):118.

21. Martínez-Zamudio RI, Roux PF, de Freitas JANLF, Robinson L, Doré G, Sun B, et al. AP-1 imprints a reversible transcriptional programme of senescent cells. Nat Cell Biol. 2020 Jul;22(7):842–55.

22. Brückmann NH, Bennedsen SN, Duijf PHG, Terp MG, Thomassen M, Larsen M, et al. A functional genetic screen identifies the Mediator complex as essential for SSX2-induced senescence. Cell Death Dis. 2019 Nov 6;10(11):1–12.

23. Tyler EJ, Gutierrez Del Arroyo A, Hughes BK, Wallis R, Garbe JC, Stampfer MR, et al. Early growth response 2 (EGR2) is a novel regulator of the senescence programme. Aging Cell. 2021 Mar;20(3):e13318.

24. Zhang C, Zhang X, Huang L, Guan Y, Huang X, Tian XL, et al. ATF3 drives senescence by reconstructing accessible chromatin profiles. Aging Cell. 2021 Mar;20(3):e13315.

25. Casella G, Munk R, Kim KM, Piao Y, De S, Abdelmohsen K, et al. Transcriptome signature of cellular senescence. Nucleic Acids Res. 2019 Aug 22;47(14):7294–305.

26. Zhao H, Darzynkiewicz Z. Biomarkers of Cell Senescence Assessed by Imaging Cytometry. Methods Mol Biol Clifton NJ. 2013;965:83–92.

27. Dimri GP, Lee X, Basile G, Acosta M, Scott G, Roskelley C, et al. A biomarker that identifies senescent human cells in culture and in aging skin in vivo. Proc Natl Acad Sci U S A. 1995 Sep 26;92(20):9363–7.

28. Kim EK, Moon S, Kim DK, Zhang X, Kim J. CXCL1 induces senescence of cancer-associated fibroblasts via autocrine loops in oral squamous cell carcinoma. PLOS ONE. 2018 Jan 23;13(1):e0188847.

29. Coppé JP, Patil CK, Rodier F, Krtolica A, Beauséjour CM, Parrinello S, et al. A Human-Like Senescence-Associated Secretory Phenotype Is Conserved in Mouse Cells Dependent on Physiological Oxygen. PLOS ONE. 2010 Feb 12;5(2):e9188.

30. Coppé JP, Desprez PY, Krtolica A, Campisi J. The senescence-associated secretory phenotype: the dark side of tumor suppression. Annu Rev Pathol. 2010;5:99–118.

31. Levi N, Papismadov N, Solomonov I, Sagi I, Krizhanovsky V. The ECM path of senescence in aging: components and modifiers. FEBS J. 2020 Jul;287(13):2636–46.

32. Sun W, Hu Y. eQTL Mapping Using RNA-seq Data. Stat Biosci. 2013 May 1;5(1):198–219.

33. Wittkopp PJ, Haerum BK, Clark AG. Evolutionary changes in cis and trans gene regulation. Nature. 2004 Jul 1;430(6995):85–8.

34. Yevshin I, Sharipov R, Kolmykov S, Kondrakhin Y, Kolpakov F. GTRD: a database on gene transcription regulation-2019 update. Nucleic Acids Res. 2019 Jan 8;47(D1):D100–5.

35. Wang Y, Sui Y, Lian A, Han X, Liu F, Zuo K, et al. PBX1 Attenuates Hair Follicle-Derived Mesenchymal Stem Cell Senescence and Apoptosis by Alleviating Reactive Oxygen Species-Mediated DNA Damage Instead of Enhancing DNA Damage Repair. Front Cell Dev Biol. 2021;9:739868.

36. Bandyopadhyay D, Okan NA, Bales E, Nascimento L, Cole PA, Medrano EE. Down-regulation of p300/CBP histone acetyltransferase activates a senescence checkpoint in human melanocytes. Cancer Res. 2002 Nov 1;62(21):6231–9.

37. Yang K, Wang F, Zhang H, Wang X, Chen L, Su X, et al. Target Inhibition of CBP Induced Cell Senescence in BCR-ABL- T315I Mutant Chronic Myeloid Leukemia. Front Oncol [Internet]. 2021 [cited 2022 Mar 10];10. Available from: https://www.frontiersin.org/article/10.3389/fonc.2020.588641

38. Qyang Y, Luo X, Lu T, Ismail PM, Krylov D, Vinson C, et al. Cell-type-dependent activity of the ubiquitous transcription factor USF in cellular proliferation and transcriptional activation. Mol Cell Biol. 1999 Feb;19(2):1508–17.

39. Pawar SA, Szentirmay MN, Hermeking H, Sawadogo M. Evidence for a cancer-specific switch at the CDK4 promoter with loss of control by both USF and c-Myc. Oncogene. 2004 Aug 12;23(36):6125–35.

40. Chen N, Szentirmay MN, Pawar SA, Sirito M, Wang J, Wang Z, et al. Tumor-suppression function of transcription factor USF2 in prostate carcinogenesis. Oncogene. 2006 Jan;25(4):579–87.

41. Aperlo C, Boulukos KE, Pognonec P. The basic region/helix-loop-helix/leucine repeat transcription factor USF interferes with Ras transformation. Eur J Biochem. 1996 Oct 1;241(1):249–53.

42. Hu D, Tjon EC, Andersson KM, Molica GM, Pham MC, Healy B, et al. Aberrant expression of USF2 in refractory rheumatoid arthritis and its regulation of proinflammatory cytokines in Th17 cells. Proc Natl Acad Sci. 2020 Dec;117(48):30639–48.

43. Redon CE, Dickey JS, Bonner WM, Sedelnikova OA. γ-H2AX as a biomarker of DNA damage induced by ionizing radiation in human peripheral blood lymphocytes and artificial skin. Adv Space Res Off J Comm Space Res COSPAR. 2009;43(8):1171–8.

44. Fumagalli M, Rossiello F, Mondello C, d'Adda di Fagagna F. Stable Cellular Senescence Is Associated with Persistent DDR Activation. PLoS ONE. 2014 Oct 23;9(10):e110969.

45. Chen JH, Ozanne SE. Deep senescent human fibroblasts show diminished DNA damage foci but retain checkpoint capacity to oxidative stress. FEBS Lett. 2006 Dec 11;580(28–29):6669–73.

46. Bakkenist CJ, Drissi R, Wu J, Kastan MB, Dome JS. Disappearance of the telomere dysfunction-induced stress response in fully senescent cells. Cancer Res. 2004 Jun 1;64(11):3748–52.

47. Siddiqui MS, François M, Fenech MF, Leifert WR. Persistent γH2AX: A promising molecular marker of DNA damage and aging. Mutat Res Rev Mutat Res. 2015 Dec;766:1–19.

48. Venkata Narayanan I, Paulsen MT, Bedi K, Berg N, Ljungman EA, Francia S, et al. Transcriptional and post-transcriptional regulation of the ionizing radiation response by ATM and p53. Sci Rep. 2017 Apr;7(1):43598.

49. Silva E, Ideker T. Transcriptional Responses to DNA Damage. DNA Repair. 2019 Jul;79:40–9.

50. Shang D, Sun D, Shi C, Xu J, Shen M, Hu X, et al. Activation of epidermal growth factor receptor signaling mediates cellular senescence induced by certain pro-inflammatory cytokines. Aging Cell. 2020 May;19(5):e13145.

51. Huang RX, Zhou PK. DNA damage response signaling pathways and targets for radiotherapy sensitization in cancer. Signal Transduct Target Ther. 2020 May 1;5(1):1–27.

52. Nickoloff JA, Boss MK, Allen CP, LaRue SM. Translational research in radiation-induced DNA damage signaling and repair. Transl Cancer Res. 2017 Jul;6(Suppl 5):S875–91.

53. Olive PL, Banáth JP. The comet assay: a method to measure DNA damage in individual cells. Nat Protoc. 2006;1(1):23–9.

54. Podhorecka M, Skladanowski A, Bozko P. H2AX Phosphorylation: Its Role in DNA Damage Response and Cancer Therapy. J Nucleic Acids. 2010 Aug 3;2010:920161.

55. Kim YM, Byun HO, Jee BA, Cho H, Seo YH, Kim YS, et al. Implications of time-series gene expression profiles of replicative senescence. Aging Cell. 2013;12(4):622–34.

56. Santoro A, Spinelli CC, Martucciello S, Nori SL, Capunzo M, Puca AA, et al. Innate immunity and cellular senescence: The good and the bad in the developmental and aged brain. J Leukoc Biol. 2018;103(3):509–24.

57. Kale A, Sharma A, Stolzing A, Desprez PY, Campisi J. Role of immune cells in the removal of deleterious senescent cells. Immun Ageing. 2020 Dec;17(1):16.

58. Basisty N, Kale A, Jeon OH, Kuehnemann C, Payne T, Rao C, et al. A proteomic atlas of senescence-associated secretomes for aging biomarker development. PLOS Biol. 2020 Jan 16;18(1):e3000599.

59. Purcell M, Kruger A, Tainsky MA. Gene expression profiling of replicative and induced senescence. Cell Cycle Georget Tex. 2014;13(24):3927–37.

60. Villarroel CA, Bastías M, Canessa P, Cubillos FA. Uncovering Divergence in Gene Expression Regulation in the Adaptation of Yeast to Nitrogen Scarcity. mSystems. 2021 Aug 31;6(4):e0046621.

61. Veyrieras JB, Kudaravalli S, Kim SY, Dermitzakis ET, Gilad Y, Stephens M, et al. High-Resolution Mapping of Expression-QTLs Yields Insight into Human Gene Regulation. PLOS Genet. 2008 Oct 10;4(10):e1000214.

62. Vierbuchen T, Ling E, Cowley CJ, Couch CH, Wang X, Harmin DA, et al. AP-1 Transcription Factors and the BAF Complex Mediate Signal-Dependent Enhancer Selection. Mol Cell. 2017 Dec 21;68(6):1067-1082.e12.

63. Heinz S, Romanoski CE, Benner C, Allison KA, Kaikkonen MU, Orozco LD, et al. Effect of natural genetic variation on enhancer selection and function. Nature. 2013 Nov;503(7477):487–92.

64. Sato AYS, Antonioli E, Tambellini R, Campos AH. ID1 inhibits USF2 and blocks TGF-β-induced apoptosis in mesangial cells. Am J Physiol Renal Physiol. 2011 Dec;301(6):F1260-1269.

65. Chi TF, Khoder-Agha F, Mennerich D, Kellokumpu S, Miinalainen Ii, Kietzmann T, et al. Loss of USF2 promotes proliferation, migration and mitophagy in a redox-dependent manner. Redox Biol. 2020 Oct 7;37:101750.

66. Vicencio JM, Galluzzi L, Tajeddine N, Ortiz C, Criollo A, Tasdemir E, et al. Senescence, apoptosis or autophagy? When a damaged cell must decide its path--a mini-review. Gerontology. 2008;54(2):92–9.

67. Childs BG, Baker DJ, Kirkland JL, Campisi J, van Deursen JM. Senescence and apoptosis: dueling or complementary cell fates? EMBO Rep. 2014 Nov;15(11):1139–53.

68. Zhang X, Li J, Sejas DP, Pang Q. The ATM/p53/p21 pathway influences cell fate decision between apoptosis and senescence in reoxygenated hematopoietic progenitor cells. J Biol Chem. 2005 May 20;280(20):19635–40.

69. Hsu CH, Altschuler SJ, Wu LF. Patterns of Early p21 Dynamics Determine Proliferation-Senescence Cell Fate after Chemotherapy. Cell. 2019 Jul 11;178(2):361-373.e12.

70. Panneer Selvam S, Roth BM, Nganga R, Kim J, Cooley MA, Helke K, et al. Balance between senescence and apoptosis is regulated by telomere damage-induced association between p16 and caspase-3. J Biol Chem. 2018 Jun 22;293(25):9784–800.

71. Lee S, Schmitt CA. The dynamic nature of senescence in cancer. Nat Cell Biol. 2019 Jan;21(1):94–101.

72. Beauséjour CM, Krtolica A, Galimi F, Narita M, Lowe SW, Yaswen P, et al. Reversal of human cellular senescence: roles of the p53 and p16 pathways. EMBO J. 2003 Aug 15;22(16):4212–22.

73. Baron Y, Corre S, Mouchet N, Vaulont S, Prince S, Galibert MD. USF-1 Is Critical for Maintaining Genome Integrity in Response to UV-Induced DNA Photolesions. PLoS Genet. 2012 Jan 26;8(1):e1002470.

74. Song X, Zhu M, Li H, Liu B, Yan Z, Wang W, et al. USF1 promotes the development of knee osteoarthritis by activating the NF-κB signaling pathway. Exp Ther Med. 2018 Oct 1;16(4):3518–24.

75. Ruuth M, Soronen J, Kaiharju E, Merikanto K, Perttilä J, Metso J, et al. USF1 deficiency alleviates inflammation, enhances cholesterol efflux and prevents cholesterol accumulation in macrophages. Lipids Health Dis. 2018 Dec 13;17:285.

76. Corre S, Galibert MD. Upstream stimulating factors: highly versatile stress-responsive transcription factors. Pigment Cell Res. 2005;18(5):337–48.

77. Bouafia A, Corre S, Gilot D, Mouchet N, Prince S, Galibert MD. p53 Requires the Stress Sensor USF1 to Direct Appropriate Cell Fate Decision. PLoS Genet. 2014 May 15;10(5):e1004309.

78. Samarakoon R, Overstreet JM, Higgins SP, Higgins PJ. TGF-β1 → SMAD/p53/USF2 → PAI-1 transcriptional axis in ureteral obstruction-induced renal fibrosis. Cell Tissue Res. 2012 Jan;347(1):117–28.

79. Dörr JR, Yu Y, Milanovic M, Beuster G, Zasada C, Däbritz JHM, et al. Synthetic lethal metabolic targeting of cellular senescence in cancer therapy. Nature. 2013 Sep;501(7467):421–5.

80. Park JT, Lee YS, Cho KA, Park SC. Adjustment of the lysosomal-mitochondrial axis for control of cellular senescence. Ageing Res Rev. 2018 Nov;47:176–82.

81. Brunk UT, Terman A. Lipofuscin: mechanisms of age-related accumulation and influence on cell function. Free Radic Biol Med. 2002 Sep 1;33(5):611–9.

82. Kurz DJ, Decary S, Hong Y, Erusalimsky JD. Senescence-associated (beta)-galactosidase reflects an increase in lysosomal mass during replicative ageing of human endothelial cells. J Cell Sci. 2000 Oct;113 (Pt 20):3613–22.

83. Lee BY, Han JA, Im JS, Morrone A, Johung K, Goodwin EC, et al. Senescence-associated beta-galactosidase is lysosomal beta-galactosidase. Aging Cell. 2006 Apr;5(2):187–95.

84. Pinheiro I, Dejager L, Petta I, Vandevyver S, Puimège L, Mahieu T, et al. LPS resistance of SPRET/Ei mice is mediated by Gilz, encoded by the Tsc22d3 gene on the X chromosome. EMBO Mol Med. 2013 Mar;5(3):456–70.

85. Vanlaere I, Vanderrijst A, Guénet JL, De Filette M, Libert C. Mx1 causes resistance against influenza A viruses in the Mus spretus-derived inbred mouse strain SPRET/Ei. Cytokine. 2008 Apr;42(1):62–70.

86. Blanchet C, Jaubert J, Carniel E, Fayolle C, Milon G, Szatanik M, et al. Mus spretus SEG/Pas mice resist virulent Yersinia pestis, under multigenic control. Genes Immun. 2011 Jan;12(1):23–30.

87. Pérez del Villar L, Vicente B, Galindo-Villardón P, Castellanos A, Pérez-Losada J, Muro A. Schistosoma mansoni experimental infection in Mus spretus (SPRET/EiJ strain) mice. Parasite. 2013;20:27.

88. Dejager L, Libert C, Montagutelli X. Thirty years of Mus spretus: a promising future. Trends Genet. 2009 May 1;25(5):234–41.

89. Khan M, Gasser S. Generating Primary Fibroblast Cultures from Mouse Ear and Tail Tissues. J Vis Exp JoVE [Internet]. 2016 [cited 2022 Mar 23];(107). Available from: https://www.ncbi.nlm.nih.gov/pmc/articles/PMC4781275/

90. Danecek P, Bonfield JK, Liddle J, Marshall J, Ohan V, Pollard MO, et al. Twelve years of SAMtools and BCFtools. GigaScience. 2021 Feb 16;10(2):giab008.

91. Langmead B, Salzberg SL. Fast gapped-read alignment with Bowtie 2. Nat Methods. 2012 Apr;9(4):357–9.

92. Li H, Handsaker B, Wysoker A, Fennell T, Ruan J, Homer N, et al. The Sequence Alignment/Map format and SAMtools. Bioinforma Oxf Engl. 2009 Aug 15;25(16):2078–9.

93. Li H. A statistical framework for SNP calling, mutation discovery, association mapping and population genetical parameter estimation from sequencing data. Bioinforma Oxf Engl. 2011 Nov 1;27(21):2987–93.

94. Kim D, Pertea G, Trapnell C, Pimentel H, Kelley R, Salzberg SL. TopHat2: accurate alignment of transcriptomes in the presence of insertions, deletions and gene fusions. Genome Biol. 2013 Apr 25;14(4):R36.

95. Putri GH, Anders S, Pyl PT, Pimanda JE, Zanini F. Analysing high-throughput sequencing data in Python with HTSeq 2.0. Bioinformatics. 2022 Mar 21;btac166.

96. Ashburner M, Ball CA, Blake JA, Botstein D, Butler H, Cherry JM, et al. Gene Ontology: tool for the unification of biology. Nat Genet. 2000 May;25(1):25–9.

97. Gene Ontology Consortium. The Gene Ontology resource: enriching a GOld mine. Nucleic Acids Res. 2021 Jan 8;49(D1):D325–34.

98. Escher C, Reiter L, MacLean B, Ossola R, Herzog F, Chilton J, et al. Using iRT, a normalized retention time for more targeted measurement of peptides. Proteomics. 2012 Apr;12(8):1111–21.

99. Gillet LC, Navarro P, Tate S, Röst H, Selevsek N, Reiter L, et al. Targeted Data Extraction of the MS/MS Spectra Generated by Data-independent Acquisition: A New Concept for Consistent and Accurate Proteome Analysis*. Mol Cell Proteomics. 2012 Jun 1;11(6):O111.016717.

100. Bruderer R, Bernhardt OM, Gandhi T, Xuan Y, Sondermann J, Schmidt M, et al. Optimization of Experimental Parameters in Data-Independent Mass Spectrometry Significantly Increases Depth and Reproducibility of Results. Mol Cell Proteomics MCP. 2017 Dec;16(12):2296–309.

101. Collins BC, Hunter CL, Liu Y, Schilling B, Rosenberger G, Bader SL, et al. Multi-laboratory assessment of reproducibility, qualitative and quantitative performance of SWATH-mass spectrometry. Nat Commun. 2017 Aug 21;8(1):291.

102. Benjamini Y, Hochberg Y. Controlling the False Discovery Rate: A Practical and Powerful Approach to Multiple Testing. J R Stat Soc Ser B Methodol. 1995;57(1):289–300.

103. Livak KJ, Schmittgen TD. Analysis of Relative Gene Expression Data Using Real-Time Quantitative PCR and the 2−ΔΔCT Method. Methods. 2001 Dec 1;25(4):402–8.

104. Gyori BM, Venkatachalam G, Thiagarajan PS, Hsu D, Clement MV. OpenComet: An automated tool for comet assay image analysis. Redox Biol. 2014 Jan 1;2:457–65.

105. Schneider CA, Rasband WS, Eliceiri KW. NIH Image to ImageJ: 25 years of image analysis. Nat Methods. 2012 Jul;9(7):671–5.

106. Roy S, Lagree S, Hou Z, Thomson JA, Stewart R, Gasch AP. Integrated Module and Gene-Specific Regulatory Inference Implicates Upstream Signaling Networks. PLOS Comput Biol. 2013 Oct 17;9(10):e1003252.